

# CHALMERS



## Analysis and modelling of an induction machine with a pulsating load torque used for a washing machine application

*Master of Science Thesis in the Master Degree Program Automation and  
Mechatronics Engineering*

MAGNUS HEDIN  
LINDA LUNDSTRÖM

Department of Energy and Environment  
*Division of Electric Power Engineering*  
CHALMERS UNIVERSITY OF TECHNOLOGY  
Göteborg, Sweden, 2007



## **Abstract**

The goal of this master thesis is to derive a model of the induction machine that drives the washing machine drum, a model for the drum with an unbalanced load and to derive a controller for the induction machine. In addition to the models, it should also be investigated if the currents, drawn by the induction machine, will vary with the unbalanced load. Finally it should be investigated if it is possible to determine the mass of the unbalanced load simply by looking at the stator currents.

A vector control drive consisting of a current and a speed PI-controller have been derived and implemented in MATLAB/Simulink. Two controllers have been derived, one equipped with a flux estimator for speed sensed control and the other with a flux and speed estimator for sensorless control. The induction machine model and the model for the washing drum with unbalanced load have been verified to work as intended. It was also found that it should be possible to measure the currents, represented in the synchronously rotating reference frame, drawn by the induction machine to determine the size of the unbalanced load.

# Preface & Acknowledgments

This paper is a Master of Science thesis in the master degree program Automation and Mechatronics Engineering. The thesis work was carried out for Asko Cylinda AB at the department of Energy and Environment at Chalmers University of Technology.

We would like to thank all of the involved persons at Asko Cylinda AB and especially Patrik Jansson who have been most helpful. We would also like to thank our tutor at school, Torbjörn Tiring, who have been helpful with ideas and suggestions in the course of this thesis work.

Magnus Hedin & Linda Lundström  
Gothenburg, April 2007

# Contents

<b>1</b>	<b>Introduction</b>	<b>4</b>
1.1	Background . . . . .	4
1.2	Purpose . . . . .	5
<b>2</b>	<b>The Washing Machine</b>	<b>6</b>
<b>3</b>	<b>Induction Machine Basics</b>	<b>7</b>
<b>4</b>	<b>Modelling</b>	<b>10</b>
4.1	Motor Model . . . . .	10
4.1.1	Equivalent Circuit Parameter Determination . . . . .	15
4.1.2	Simulink Implementation . . . . .	15
4.2	Drum and Transmission Model . . . . .	16
4.2.1	Simulink implementation . . . . .	18
<b>5</b>	<b>Controller Design</b>	<b>19</b>
5.1	Different Controller Methods . . . . .	20
5.1.1	Volt/Hertz control . . . . .	20
5.1.2	Vector control . . . . .	20
5.1.3	Direct Torque Control (DTC) . . . . .	21
5.2	Inverse- $\Gamma$ Model . . . . .	21
5.3	Current Controller . . . . .	23
5.3.1	Active Damping . . . . .	25
5.3.2	Back Calculation . . . . .	25
5.3.3	Simulink Implementation . . . . .	26
5.4	Speed Controller . . . . .	26
5.4.1	Active Damping . . . . .	27
5.4.2	Back Calculation . . . . .	28
5.4.3	Simulink Implementation . . . . .	28
5.5	Flux Sensorless Control . . . . .	29
5.5.1	Simulink Implementation . . . . .	29
5.6	Speed and Flux Sensorless Control . . . . .	29
5.6.1	Speed Estimation . . . . .	30
5.6.2	Flux Estimation . . . . .	30

5.6.3	Simulink Implementation . . . . .	32
<b>6</b>	<b>Verification</b>	<b>34</b>
6.1	Induction Machine . . . . .	34
6.1.1	T-Equivalent Circuit Parameters . . . . .	34
6.1.2	Direct Start Measurements . . . . .	34
6.1.3	Induction Machine With Unbalanced Load . . . . .	37
6.2	Drum . . . . .	40
6.3	Current and Speed Controller . . . . .	41
6.3.1	Flux Sensorless and Speed Sensored Control . . . . .	41
6.3.2	Flux and Speed Sensorless Control . . . . .	41
<b>7</b>	<b>Conclusion</b>	<b>43</b>
<b>8</b>	<b>Further Work</b>	<b>44</b>
	<b>Nomenclature</b>	<b>45</b>
<b>A</b>	<b>Reference Frame Theory</b>	<b>50</b>
A.1	Stationary Circuit Element . . . . .	51
A.2	Rotating Circuit Element . . . . .	54
<b>B</b>	<b>DC Resistance Test</b>	<b>55</b>
<b>C</b>	<b>No-Load Test</b>	<b>56</b>
<b>D</b>	<b>Locked Rotor Test</b>	<b>59</b>
<b>E</b>	<b>Direct Start</b>	<b>61</b>
<b>F</b>	<b>Torque-Speed Test</b>	<b>63</b>
<b>G</b>	<b>Induction Machine Parameters</b>	<b>64</b>

# Chapter 1

## Introduction

Asko Cylinda AB was founded in 1950 as one of many washing machine manufacturer but are today one of two Swedish washing machine manufacturer on the market. Even in 1950 most of the washing machines were equipped with spin ability, and is still one area in which improvements can be made. Currently, washing machine manufacturers are aiming to minimize vibrations in order to increase the spin speed.

### 1.1 Background

A complicated process in washing machines is the spinning process where excess water in the laundry is to be removed. In order to do this fast and efficient, a high drum-speed is desired. If the laundry is unevenly distributed the drum becomes unbalanced and a high speed can not be obtained because of the vibrations. One way to balance the drum is to redistribute the laundry by alternating between clockwise and counter-clockwise rotation of the drum. This, however does not improve the performance as much as needed for the high speeds that are of interest here. Another possibility, suggested by Asko Cylinda, is to have some mechanics to balance the drum which requires information of the position and the mass of the unbalanced load. An interesting approach would be to try to use the variation of the currents in the induction machine to obtain information about how the laundry is distributed.

The modeling of the induction machine can be approached in different ways. One way is to use the T-equivalent expressed in the arbitrary reference frame [6]. When it comes to the controller, it is more convenient to express the induction machine with the inverse- $\Gamma$  equivalent circuit.

## 1.2 Purpose

The purpose with this master thesis work is to build and implement a mathematical model of the induction machine and the washing drum in MATLAB/Simulink. An important goal is also to implement the unbalanced load and in particular to obtain the load torque acting on the induction machine from the unbalanced load. Finally it should be investigated if the mass and the position of the unbalanced load can be determined from the variation of the currents that drives the induction machine.

## Chapter 2

# The Washing Machine

The part of the washing machine, that is of interest for this master thesis, mainly consists of a user interface, a controller, a converter and an electric motor connected to the washing drum by a belt as shown in Figure 2.1.

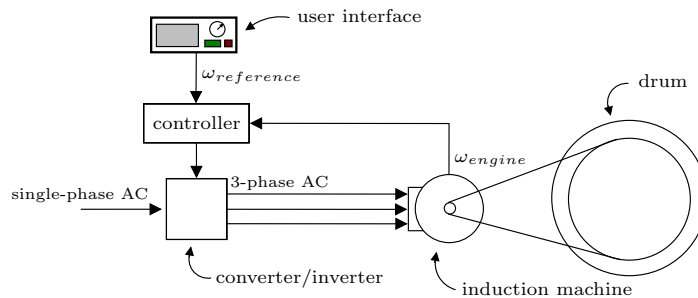


Figure 2.1: Schematic view of the construction of a washing machine.

The washing machine is supplied with a single-phase 230V AC source but the motor is a 3-phase induction machine. To supply the induction machine with a 3-phase variable frequency current a converter is used. The converter is governed by the controller which calculates the appropriate voltage and frequency from the actual or estimated rotor speed and the reference speed set by the user interface unit. The objective for the controller is to make sure that the speed of the induction machine follows the reference speed set by the user interface.

The load torque on the motor shaft is not only dependent on the inertia of the drum but also on the mass and location of the laundry inside the drum. If the laundry is unevenly distributed inside the drum it will be unbalanced and cause the torque on the induction machine output shaft to vary with the angular location of the drum.

## Chapter 3

# Induction Machine Basics

The motor, used in this thesis work, is a two pole induction machine composed of a cage rotor and a stator containing windings connected to the 3-phase power supply.

In common for induction machines is that the stator is made up of a stack of steel laminations pressed into a aluminum or cast iron frame, and that the rotor consists of a stack of steel laminations with evenly spaced slots punched around the circumference where the rotor bars are placed, see Figure 3.1. Both the rotor and stator lamination plates are insulated to prevent *eddy currents*<sup>1</sup> from flowing in the iron. The rotor slots are also skewed to reduce non-linear effect such as harmonics and torque pulsation.

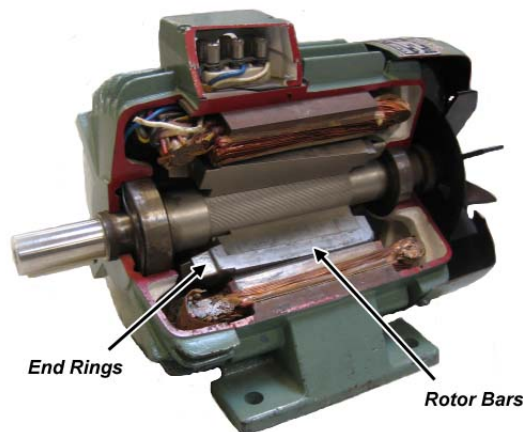


Figure 3.1: Inside view of an induction machine.

---

<sup>1</sup>An eddy current is an electrical phenomenon and is caused when a moving magnetic field intersects a conductor. The relative motion causes a circulating flow of electrons, or current, within the conductor. These circulating eddies of current create electromagnets with magnetic fields that oppose the effect of the applied magnetic field according to Lenz's law.

### The Stator

Each of the three alternating currents that flows in the three stator windings give rise to a magnetic field. Since the currents are alternating, the resultant magnetic field (see Figure 3.2a) rotates with the stator current frequency and crosses the air-gap radially. It is the layout of the stator windings that determines the number of poles, see Figure 3.2b and hence the speed of the rotating magnetic field in relation to the supply frequency.

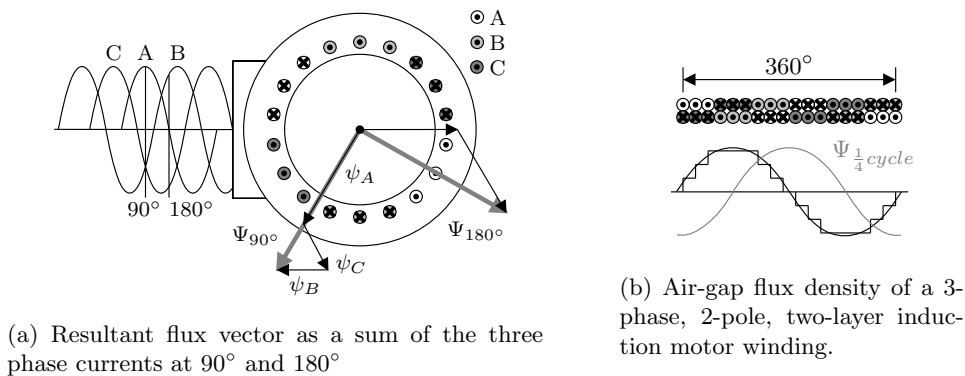


Figure 3.2: Setup of the air-gap flux wave  $\Psi$ .

Since every stator conductor is cut by the rotating magnetic field an alternating electromotive force (emf)  $E$  will be induced opposing the voltage  $V$  according to Lenz's law. The stator can thus be described by the equation  $V = I_m R + E$ , which shows the relation between the applied voltage  $V$ , the magnetizing current  $I_m$  (i.e. the current that sets up the flux) and the induced emf  $E$ . If the flux decreases, so will the emf. This makes the magnetizing current increase which in turn makes the flux increase and hence the emf. The magnetizing current will adjust itself so that the emf always equals the applied voltage.

### The Rotor

Torque producing currents are induced in the rotor bars by interaction with the air-gap flux wave, *the rotor is dragged along by the rotating field*. If the rotor is held stationary there will be a high current induced in the rotor bars since the wave will cut the bars at a high velocity. If, on the other hand, the rotor is rotating with the same velocity as the magnetic field, there will be no current induced in the rotor bars. The slip is defined as the relative velocity between the speed of the magnetic field ( $n_s$ ), which is also known as the synchronous speed, and the speed of the rotor ( $n$ ), i.e.

$$s = \frac{n_s - n}{n_s}. \quad (3.1)$$

If a mechanical load is applied to the shaft, the rotor slows down, the slip increases and more current gets induced in the rotor bars. This results in a stronger magnetic field in the rotor bars and hence a higher torque is produced. The currents in the rotor bars also sets up an magnetomotive force (mmf) wave in the stator that counteracts with the stator generated flux wave. Hence, a modest reduction of air-gap flux results in a reduction of e.m.f. Since the applied voltage is constant this increases the magnetizing current.

### Torque Production

With a small slip, the frequency of the induced emf in the rotor is low which makes the reactance of the rotor low (in this case the rotor is predominantly resistive) and thus the rotor current in phase with the rotor emf which in turn is in phase with the air-gap flux. As a result the torque-speed relationship for small slip is approximately a straight line (AB in Figure 3.3).

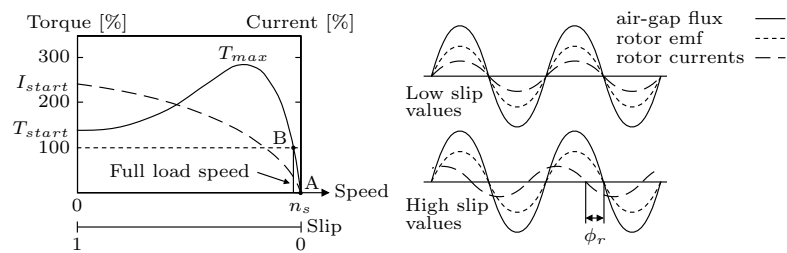


Figure 3.3: Torque speed relationship.

As the slip increases, both the rotor emf and frequency increases. With increased frequency the rotor inductive reactance also increases which makes the current lag by a angle  $\phi_r$  shown in the right part of Figure 3.3.

# Chapter 4

## Modelling

In this chapter a model of the induction machine is derived together with a model of the drum and the unbalanced load. The induction machine is represented mathematically using the two-axis theory of electric machines. The two-phase signal representation is often used to reduce the complexity of the differential equations that describes the induction machine [6]. In this thesis the stationary ( $\alpha\beta$ ) reference frame will be used when modeling the induction machine since all voltages are assumed to be balanced and continuous, see Appendix A. The synchronously rotating ( $dq$ ) reference frame is used when deriving the controllers, see Section 5, since all  $dq$  signals are DC and hence easy to control. A description of the different reference frames used in this thesis can be found in Appendix A.

Also in this chapter, a description of how the models have been implemented in MATLAB/Simulink is given.

### 4.1 Motor Model

The induction machine considered in this thesis will be assumed to be symmetrical, which implies that the rotor resistances are equal for each winding.

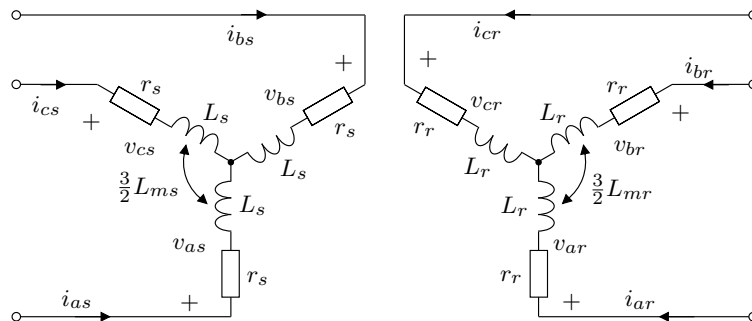


Figure 4.1: Induction machine winding in stator and rotor.

From the law of induction it follows that the part of the applied voltage which is not lost as heat in the stator windings (i.e. stator resistance) will build up a flux wave in the stator windings. With  $\mathbf{v}_{abcs}$  as the applied voltage space vector,  $\mathbf{i}_{abcs}$  as the stator current and  $\Psi_{abcs}$  as the stator flux linkage, where the subscript  $s$  implies stator coordinates. With the rotor described in a similar way, the voltage equations for the induction machine can be written as

$$\mathbf{v}_{abcs} = \mathbf{r}_s \mathbf{i}_{abcs} + \frac{d\Psi_{abcs}}{dt} \quad (4.1)$$

$$\mathbf{v}_{abcr} = \mathbf{r}_r \mathbf{i}_{abcr} + \frac{d\Psi_{abcr}}{dt} \quad (4.2)$$

where  $\Psi_{abcs}$  and  $\Psi_{abcr}$  are the stator and rotor flux linkages respectively and where

$$\mathbf{f}_{abcs} = [ f_{as} \quad f_{bs} \quad f_{cs} ]^T \quad (4.3)$$

$$\mathbf{f}_{abcr} = [ f_{ar} \quad f_{br} \quad f_{cr} ]^T \quad (4.4)$$

where  $\mathbf{f}$  represents current, voltage or flux linkage. Referring the rotor variables to the stator side, (4.2) can be written as

$$\mathbf{v}'_{abcr} = \mathbf{r}'_r \mathbf{i}'_{abcr} + \frac{d\Psi'_{abcr}}{dt} \quad (4.5)$$

where the transformed variables either is the ratio of the number of stator windings,  $N_s$ , to the number of rotor windings,  $N_r$ , or reversed. The following yields

$$\mathbf{v}'_{abcr} = \frac{N_s}{N_r} \mathbf{v}_{abcr}, \quad \mathbf{i}'_{abcr} = \frac{N_r}{N_s} \mathbf{i}_{abcr}, \quad \Psi'_{abcr} = \frac{N_s}{N_r} \Psi_{abcr} \quad (4.6)$$

and

$$\mathbf{r}'_r = \left( \frac{N_s}{N_r} \right)^2 \mathbf{r}_r, \quad L'_{lr} = \left( \frac{N_s}{N_r} \right)^2 L_{lr}. \quad (4.7)$$

A change of variables is often used to reduce the complexity of the differential equations describing the induction machine [6]. Using the transformations described in Appendix A, and especially (A.11), the induction machine variables in (4.1) and (4.5) can be referred to a frame of reference that rotates at an arbitrary angular velocity. From this general transformation it is easy to obtain the desired transformation simply by assigning the speed of the rotation of the reference frame. Expressing (4.1) and (4.5) in the arbitrary reference frame yields

$$\mathbf{v}_{xy0s} = \mathbf{r}_s \mathbf{i}_{xy0s} + \omega \Psi_{yxs} + \frac{d\Psi_{xy0s}}{dt} \quad (4.8)$$

$$\mathbf{v}'_{xy0r} = \mathbf{r}'_r \mathbf{i}'_{xy0r} + (\omega - \omega_r) \Psi'_{yxr} + \frac{d\Psi'_{xy0r}}{dt} \quad (4.9)$$

where

$$\mathbf{f}_{xy0s} = [ f_{xs} \quad f_{ys} \quad f_{0s} ]^T \quad (4.10)$$

$$\mathbf{f}'_{xy0r} = [ f'_{xr} \quad f'_{yr} \quad f'_{0r} ]^T \quad (4.11)$$

$$\Psi_{yxs} = [ -\psi_{ys} \quad \psi_{xs} \quad 0 ]^T \quad (4.12)$$

$$\Psi'_{yxr} = [ -\psi'_{yr} \quad \psi'_{xr} \quad 0 ]^T. \quad (4.13)$$

The equation describing the flux linkages can be found by combining (A.23) with (A.21). Flux linkage as a function of current is thus given by

$$\begin{bmatrix} \psi_{xy0s} \\ \psi'_{xy0r} \end{bmatrix} = \begin{bmatrix} \mathbf{K}_s \mathbf{L}_s (\mathbf{K}_s)^{-1} & \mathbf{K}_s \mathbf{L}'_{sr} (\mathbf{K}_r)^{-1} \\ \mathbf{K}_r (\mathbf{L}'_{sr})^T (\mathbf{K}_s)^{-1} & \mathbf{K}_r \mathbf{L}'_r (\mathbf{K}_r)^{-1} \end{bmatrix} \begin{bmatrix} \mathbf{i}_{xy0s} \\ \mathbf{i}'_{xy0r} \end{bmatrix}. \quad (4.14)$$

Using the transformation matrices defined in appendix A, the matrix elements in (4.14) is found to be

$$\mathbf{K}_s \mathbf{L}_s (\mathbf{K}_s)^{-1} = \begin{bmatrix} L_{ls} + L_m & 0 & 0 \\ 0 & L_{ls} + L_m & 0 \\ 0 & 0 & L_{ls} \end{bmatrix} \quad (4.15)$$

$$\mathbf{K}_r \mathbf{L}'_r (\mathbf{K}_r)^{-1} = \begin{bmatrix} L'_{lr} + L_m & 0 & 0 \\ 0 & L'_{lr} + L_m & 0 \\ 0 & 0 & L'_{lr} \end{bmatrix} \quad (4.16)$$

$$\mathbf{K}_s \mathbf{L}'_{sr} (\mathbf{K}_r)^{-1} = \mathbf{K}_r (\mathbf{L}'_{sr})^T (\mathbf{K}_s)^{-1} = \begin{bmatrix} L_m & 0 & 0 \\ 0 & L_m & 0 \\ 0 & 0 & 0 \end{bmatrix} \quad (4.17)$$

where  $L_m$  is the magnetizing inductance given by

$$L_m = \frac{3}{2} L_{ms} = \frac{3}{2} L_{mr} \quad (4.18)$$

where  $L_{ms}$  is the stator magnetizing inductance and  $L_{mr}$  is the rotor magnetizing inductance.

Using (4.8) and (4.9) the voltage equations can be written in expanded form as

$$v_{xs} = r_s i_{xs} - \omega \psi_{ys} + p \psi_{xs} \quad (4.19)$$

$$v_{ys} = r_s i_{ys} + \omega \psi_{xs} + p \psi_{ys} \quad (4.20)$$

$$v_{0s} = r_s i_{0s} + p \psi_{0s} \quad (4.21)$$

$$v'_{xr} = r'_r i'_{xr} - (\omega - \omega_r) \psi'_{yr} + p \psi'_{xr} \quad (4.22)$$

$$v'_{yr} = r'_r i'_{yr} + (\omega - \omega_r) \psi'_{xr} + p \psi'_{yr} \quad (4.23)$$

$$v'_{0r} = r'_r i'_{0r} + p \psi'_{0r} \quad (4.24)$$

where  $p$  has replaced the operator  $d/dt$ . Since there is no voltage applied to the rotor  $v'_{xr}$ ,  $v'_{yr}$  and  $v'_{0r}$  in (4.22), (4.23) and (4.24) respectively is set to zero.

Expanding (4.14), flux linkage as a function of current is determined to

$$\psi_{xs} = L_{ls}i_{xs} + L_m(i_{xs} + i'_{xr}) \quad (4.25)$$

$$\psi_{ys} = L_{ls}i_{ys} + L_m(i_{ys} + i'_{yr}) \quad (4.26)$$

$$\psi_{0s} = L_{ls}i_{0s} \quad (4.27)$$

$$\psi'_{xr} = L'_{lr}i'_{xr} + L_m(i_{xs} + i'_{xr}) \quad (4.28)$$

$$\psi'_{yr} = L'_{lr}i'_{yr} + L_m(i_{ys} + i'_{yr}) \quad (4.29)$$

$$\psi'_{0r} = L'_{lr}i'_{0r}. \quad (4.30)$$

The voltage and flux linkage equations can also be represented with the equivalent circuit shown in Figure 4.2.

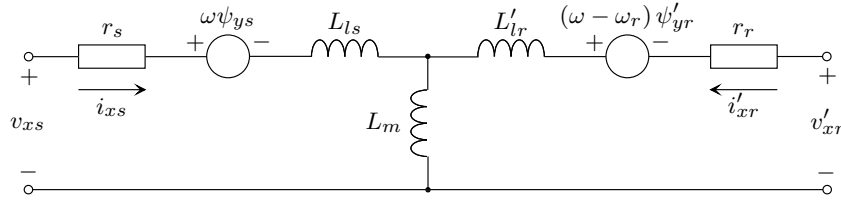


Figure 4.2:  $x$ -axis equivalent circuit in the arbitrary reference frame.

Currents can instead be expressed as a function of flux linkage yielding

$$i_{xs} = \frac{1}{L_{ls}}(\psi_{xs} - \psi_{mx}) \quad (4.31)$$

$$i_{ys} = \frac{1}{L_{ls}}(\psi_{ys} - \psi_{my}) \quad (4.32)$$

$$i_{0s} = \frac{1}{L_{ls}}\psi_{0s} \quad (4.33)$$

$$i_{xr} = \frac{1}{L'_{lr}}(\psi'_{xr} - \psi_{mx}) \quad (4.34)$$

$$i_{yr} = \frac{1}{L'_{lr}}(\psi'_{yr} - \psi_{my}) \quad (4.35)$$

$$i_{0r} = \frac{1}{L'_{lr}}\psi'_{0r} \quad (4.36)$$

where

$$\psi_{mx} = \frac{1}{\frac{1}{L_m} + \frac{1}{L_{ls}} + \frac{1}{L'_{lr}}} \left( \frac{\psi_{xs}}{L_{ls}} + \frac{\psi'_{xr}}{L'_{lr}} \right) \quad (4.37)$$

$$\psi_{my} = \frac{1}{\frac{1}{L_m} + \frac{1}{L_{ls}} + \frac{1}{L'_{lr}}} \left( \frac{\psi_{ys}}{L_{ls}} + \frac{\psi'_{yr}}{L'_{lr}} \right). \quad (4.38)$$

Inserting (4.31) - (4.36) into voltage equations (4.19) - (4.24) and rearranging, flux linkage as a function of voltage is found to be

$$\frac{d\psi_{xs}}{dt} = v_{xs} - \omega\psi_{ys} + \frac{r_s}{L_{ls}}(\psi_{mx} - \psi_{xs}) \quad (4.39)$$

$$\frac{d\psi_{ys}}{dt} = v_{ys} + \omega\psi_{xs} + \frac{r_s}{L_{ls}}(\psi_{my} - \psi_{ys}) \quad (4.40)$$

$$\frac{d\psi_{0s}}{dt} = v_{0s} - \frac{r_s}{L_{ls}}\psi_{0s} \quad (4.41)$$

$$\frac{d\psi'_{xr}}{dt} = v_{qr} - (\omega - \omega_r)\psi'_{yr} + \frac{r'_r}{L'_{lr}}(\psi_{mx} - \psi'_{xr}) \quad (4.42)$$

$$\frac{d\psi'_{yr}}{dt} = v_{dr} + (\omega - \omega_r)\psi'_{xr} + \frac{r'_r}{L'_{lr}}(\psi_{my} - \psi'_{yr}) \quad (4.43)$$

$$\frac{d\psi'_{0r}}{dt} = v_{0r} - \frac{r'_r}{L'_{lr}}\psi'_{0r}. \quad (4.44)$$

The electrical rotor speed,  $\omega_r$ , is given by

$$\frac{d\omega_r}{dt} = \frac{P}{2J}(T_e - T_{load}) \quad (4.45)$$

where  $P$  is the number of poles,  $T_{load}$  is the load torque described in section 4.2 and  $T_e$  the electrical torque given by

$$T_e = \left(\frac{3}{2}\right) \left(\frac{P}{2}\right) (\psi'_{xr}i'_{yr} - \psi'_{ys}i'_{xr}). \quad (4.46)$$

Transforming the above defined electrical speed to mechanical angular speed ( $\omega_{mech}$  in [rad/s]) or speed ( $n_{mech}$  in [rpm]) on rotor output shaft yields

$$\omega_{mech} = \frac{2}{P}\omega_r \quad (4.47)$$

$$n_{mech} = \frac{60}{2\pi}\omega_{mech}. \quad (4.48)$$

### 4.1.1 Equivalent Circuit Parameter Determination

From [8] we can learn that to determine the parameters of the induction machine equivalent circuit a few tests have to be performed. Presented below is a list with the tests together with a short description and a reference to the adequate appendix where a complete description can be found.

- *DC Resistance Test* - Appendix B. Determines the stator winding resistance  $r_s$ .
- *No-Load Test* - Appendix C. Performed to find the magnetizing impedance ( $r_c$  and  $X_m$ ) and hence the stator losses.
- *Locked Rotor Test* - Appendix D. Provides information about leakage impedances  $X_{ls}$  and  $X_{lr}$  and rotor resistance  $r_r$ . It can also be used to determine the current and torque at start as well as copper loss at full load.

To be able to verify the induction machine model a few more tests have to be performed. The purpose of these tests are to gather information about the induction machine behavior during transients but also during steady state conditions. The *Direct Start Test* gives information about the transient response and are further explained in appendix E. To get information about the steady state behavior a *Torque-Speed Test* is performed, this is explained in appendix F. The data collected from these tests are later compared with data from the model collected during the simulations.

### 4.1.2 Simulink Implementation

Flux linkage equation (4.39) - (4.44), (4.37) and (4.38), current equation (4.31) - (4.36) together with speed and torque equation (4.45) and (4.46) respectively gives the MATLAB/Simulink implemented induction machine. Below, in Figure 4.3, is a block diagram showing the connections between the equations.

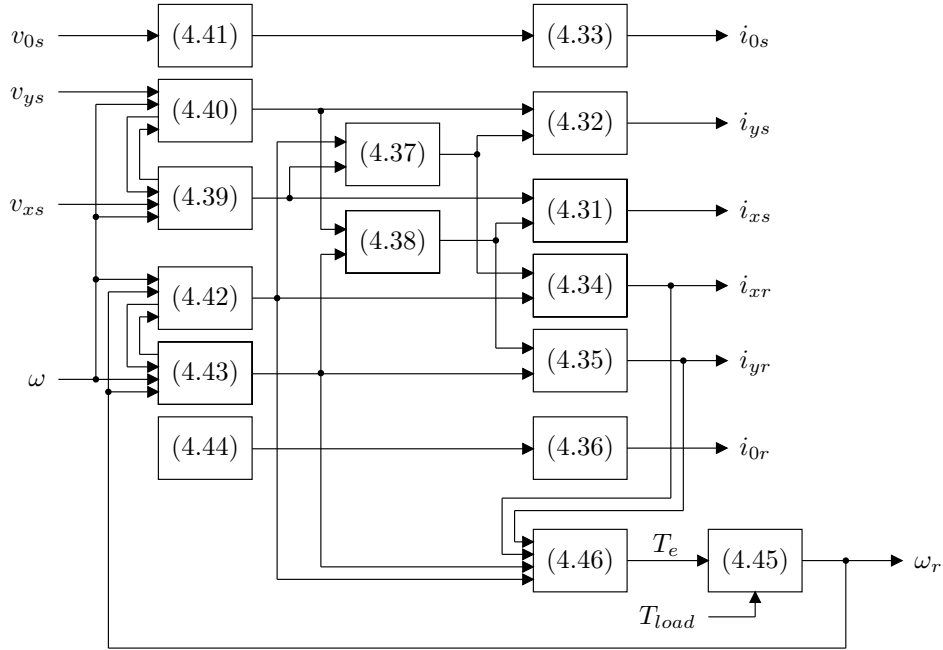


Figure 4.3: Induction machine implementation in MATLAB/Simulink.

The induction machine is modeled in the stationary ( $\alpha\beta$ ) reference frame which, according to Table A.1 in Appendix A, sets  $\omega$  to zero.

## 4.2 Drum and Transmission Model

This model describes the load torque acting on the motor shaft (i.e. the engine load torque). If the laundry is uneven distributed in the drum the center of gravity will be outside the center point of the drum, see Figure 4.4.

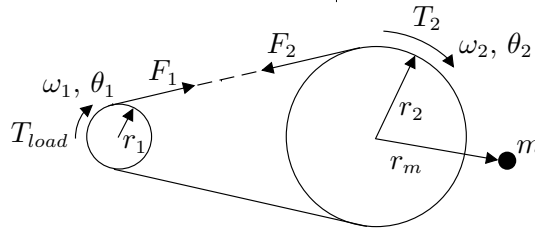


Figure 4.4: Drum model with unbalanced load.

The output torque  $T_{load}$  can be expressed as

$$T_{load} = T_1 + T_{J_1} + T_{\mu_1} \quad (4.49)$$

where

$$T_1 = F_1 r_1 \quad (4.50)$$

$$T_{J_1} = \frac{d\omega_1}{dt} J_1 \quad (4.51)$$

$$T_{\mu_1} = \mu_1 \omega_1 \quad (4.52)$$

where  $F_1$  is the belt force,  $r_1$  is the radius of the output shaft,  $\omega_1$  is the mechanical rotor speed,  $\mu_1$  is the friction coefficient for the rotor and  $J_1$  is the inertia of the rotor and rotor pulley. The belt force is given by

$$F_k = \xi r_1 \theta_1 - \xi r_2 \theta_2 + d(\omega_1 r_1 - \omega_2 r_2) \quad (k = 1, 2) \quad (4.53)$$

where  $\xi$  is the belt spring constant,  $r_2$  is the radius of the drum and  $d$  is the belt damping constant. Inserting (4.50), (4.51) and (4.53) in (4.49) yields

$$T_{load} = \xi r_1^2 \theta_1 - \xi r_1 r_2 \theta_2 + r_1 d(\omega_1 r_1 - \omega_2 r_2) + \frac{d\omega_1}{dt} J_1 + \mu_1 \omega_1. \quad (4.54)$$

The force generated on the pulley belt from the drum is not entirely due to the inertia but also dependent on the mass of the unbalanced load and the radius at which it is located from the center of the pulley. The equations for the drum can be written as

$$T_2 = T_{J_2} + T_{\mu_2} + T_{ub} \quad (4.55)$$

where the torque from the belt  $T_2$ , the torque due to the inertia  $T_{J_2}$ , the friction torque  $T_{\mu_2}$  and the torque generated by the unbalanced load  $T_{ub}$  is found using

$$T_2 = F_2 r_2 \quad (4.56)$$

$$T_{J_2} = \frac{d\omega_2}{dt} J_2 \quad (4.57)$$

$$T_{\mu_2} = \mu_2 \omega_2 \quad (4.58)$$

$$T_{ub} = \underbrace{\frac{d\omega_2}{dt} m r_m^2}_{inertia} + \underbrace{r_m m g \cos(\theta_2)}_{unbalance} \quad (4.59)$$

where  $F_2$  is given by (4.53),  $\omega_2$  is the speed of the drum,  $J_2$  is the inertia of the drum,  $\mu_2$  is the friction coefficient of the drum,  $g$  is the gravitational constant,  $r_m$  is the distance from the center of the drum to the unbalanced load and  $m$  is the mass of the unbalanced load. Inserting (4.53) and (4.56) - (4.59) into (4.55) yields

$$\frac{d\omega_2}{dt} (J_2 + m r_m^2) = \xi r_1 r_2 \theta_1 - \xi r_2^2 \theta_2 + d r_2 (\omega_1 r_1 - \omega_2 r_2) - r_m m g \cos(\theta_2) - \mu_2 \omega_2. \quad (4.60)$$

### 4.2.1 Simulink implementation

The engine load torque  $T_{load}$  is found using (4.54) and (4.60) as shown in Figure 4.5, which also is the model used in simulink.

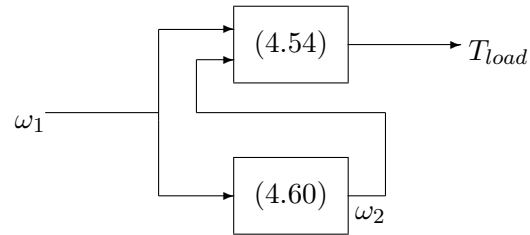


Figure 4.5: Block diagram of drum and transmission model.

# Chapter 5

## Controller Design

As already mentioned in Chapter 2, the washing program sets the desired speed of the drum. This calls for a two-loop control of the induction machine, which consists of an inner feedback loop to control the current (and hence the torque) and an outer loop to control the speed. To find a more suitable model for controller design, the dynamic inverse- $\Gamma$  model in the synchronous ( $dq$ ) coordinates is derived. It is assumed that the coordinate system is aligned with the rotor flux (perfect field orientation) which makes the stator current components  $i_{ds}$  and  $i_{qs}$  correspond to the magnetizing and armature currents, respectively, of a DC motor. With all quantities DC it is sufficient for the controllers to be of proportional-integral (PI) type.

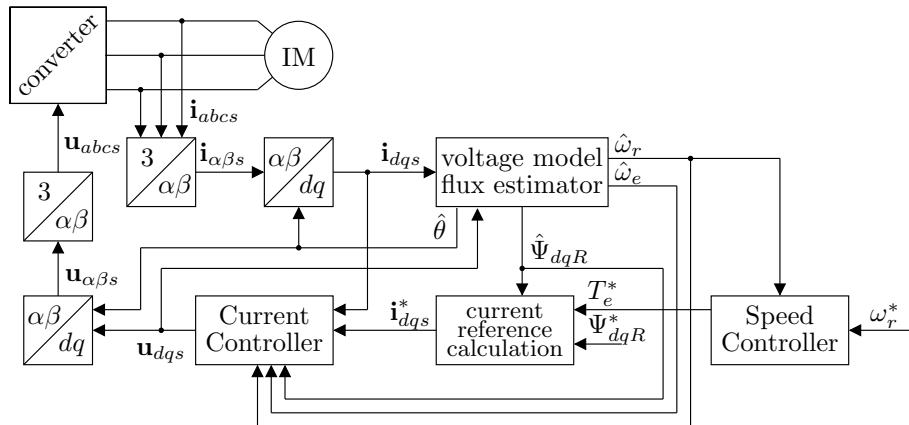


Figure 5.1: Sensorless control of induction machine using the SCVM in IFO model.

Depending on the number of sensors and what kind of sensor, different controller methods are used, of which some are described in Section 5.1. In this thesis, both a flux sensorless, which requires a speed sensor, and a speed sensorless, which require the flux and speed to be estimated, control of the

induction machine are examined. A block diagram of a statistically compensated voltage model (SCVM) flux estimator in indirect field orientation (IFO) with current and speed controller is seen in Figure 5.1. This is one of the models that is implemented in MATLAB/Simulink.

In field-oriented control the rotor flux is established in a known position, usually the d-axis of the transformation. The current are then placed in the orthogonal q-axis where it will be most effective in producing torque [5].

## 5.1 Different Controller Methods

With inspiration from [5], [9] and [10] this section briefly describes some of the available controller methods and there characteristic.

### 5.1.1 Volt/Hertz control

Volt/Hertz control in its simplest form takes a speed reference command from an external source and varies the voltage and frequency applied to the motor. By maintaining a constant V/Hz ratio, the drive can control the speed of the connected motor. This is a open-loop control strategy and neither current nor speed measurement is needed. However, there are several drawbacks. A step in reference speed is similar to the starting of the machine which will result in large peeks in the stator currents. Furthermore, the transients for speed and torque are quite slow.

### 5.1.2 Vector control

When quick torque response is highly important, vector control is the preferred controller method. Vector control relies on field orientation in which the torque is controlled simply by changing the stator current  $i_q$  and the flux by changing  $i_d$ . This method gives good transient performance by mimicking the DC motor. This can be done since the induction machine in principle is a DC machine turned inside out.

#### Flux-sensored Control

When using a flux sensor, the induction machine is not much more difficult to control than a DC machine. However the flux sensors is delicate and expensive and this is not a realistic alternative in reality.

#### Flux-sensorless Speed-sensored Control

This is the typical situation in many induction machine drives. When the speed is measured, the flux angle can be estimated with good accuracy as described in Section 5.6. The performance is comparable with the flux-sensored but the controller is more complicated.

### Flux and Speed Sensorless Control

Regarding cost and robustness this is the ideal situation. At nominal speed the flux angle can be estimated with good accuracy and hence the performance is comparable with that of the flux sensor control method. However, a major drawback is that stability and accuracy is difficult to guarantee at low speeds.

#### 5.1.3 Direct Torque Control (DTC)

This is the latest technology and according to [9] DTC only measures current and voltage to estimate the instantaneous stator flux and output torque by means of an induction machine model. Furthermore in [10] it is stated that DTC have a faster speed and torque response than ordinary AC drives and also a better static speed accuracy.

## 5.2 Inverse- $\Gamma$ Model

The use of complex vector notation simplifies the model of an AC machine from a multiple-input/multiple-output system to a single-input/single-output complex vector system. So, not taking into consideration the zero sequence components and taking  $x$ ,  $\alpha$  and  $d$  as the real axis and  $y$ ,  $\beta$  and  $q$  as the imaginary axis in complex vector notation, the rotor and stator voltage equation in the arbitrary reference frame, (4.8) and (4.9), can alternatively be expressed as

$$\mathbf{v}_{xys} = \mathbf{r}_s \mathbf{i}_{xys} + j\omega \boldsymbol{\psi}_{xys} + p\boldsymbol{\psi}_{xys} \quad (5.1)$$

$$0 = \mathbf{r}_r \mathbf{i}_{xyr} + j(\omega - \omega_r) \boldsymbol{\psi}_{xyr} + p\boldsymbol{\psi}_{xyr} \quad (5.2)$$

where

$$\mathbf{f}_{xys} = f_{xs} + jf_{ys} \quad (5.3)$$

$$\mathbf{f}_{xyr} = f_{xr} + jf_{yr} \quad (5.4)$$

where  $f$  represents voltage, current or flux linkage. The same equation holds for both the  $\alpha\beta$  and the  $dq$  system.

Expressing the rotor and stator voltage (5.1) and (5.2) in the stationary reference frame, see Table A.1 on page 50, and rearranging yields

$$p\boldsymbol{\psi}_{\alpha\beta s} = \mathbf{v}_{\alpha\beta s} - \mathbf{r}_s \mathbf{i}_{\alpha\beta s} \quad (5.5)$$

$$p\boldsymbol{\psi}_{\alpha\beta r} = j\omega_r \boldsymbol{\psi}_{\alpha\beta r} - \mathbf{r}_r \mathbf{i}_{\alpha\beta r}. \quad (5.6)$$

The inverse- $\Gamma$  model is a representation of the induction machine with the rotor leakage inductance,  $L_{lr}$ , eliminated and instead referred to the stator side. This is possible since there is a linear dependency of currents,

i.e. the magnetizing current can be expressed as the sum of the rotor and stator current.

Defining  $\Psi'_{\alpha\beta R} = a\Psi'_{\alpha\beta r}$  and  $\mathbf{i}'_{\alpha\beta R} = \mathbf{i}'_{\alpha\beta r}/a$ , flux linkage (4.25), (4.26), (4.28) and (4.29) can be written, in the complex form, as

$$\Psi_{\alpha\beta s} = (L_{ls} + L_M) i_{\alpha\beta s} + aL_M i'_{\alpha\beta R} \quad (5.7)$$

$$\Psi'_{\alpha\beta R} = aL_M i_{\alpha\beta s} + a^2 (L'_{lr} + L_M) i'_{\alpha\beta R}. \quad (5.8)$$

With equal coefficients for the stator and rotor currents in (5.8) the inductance on the rotor side can be eliminated. So, with  $a = L_M (L'_{lr} + L_M)$  (5.7) and (5.8) can now be expressed as

$$\begin{aligned} \Psi_{\alpha\beta s} &= (L_{ls} + L_M) i_{\alpha\beta s} + \frac{L_M^2}{(L'_{lr} + L_M)} i'_{\alpha\beta R} = \\ &= L_\sigma i_{\alpha\beta s} + L_M i'_{\alpha\beta R} \end{aligned} \quad (5.9)$$

$$\Psi'_{\alpha\beta R} = \frac{L_M^2}{(L'_{lr} + L_M)} (i_{\alpha\beta s} + i'_{\alpha\beta R}) = L_M i_{\alpha\beta M} \quad (5.10)$$

where  $L_s = L_{ls} + L_m$ ,  $L'_r = L'_{lr} + L_m$ ,  $L_M = L_m^2/L'_r$  and  $L_\sigma = L_s - L_M$ .

With  $r'_R = (L_m/L'_r)^2 r'_r$  the stator and rotor equations (5.5) and (5.6) can be expressed as

$$p\Psi_{\alpha\beta s} = \mathbf{v}_{\alpha\beta s} - \mathbf{r}_s \mathbf{i}_{\alpha\beta s} \quad (5.11)$$

$$p\Psi'_{\alpha\beta R} = j\omega_r \Psi'_{\alpha\beta R} - \mathbf{r}'_R \mathbf{i}'_{\alpha\beta R}. \quad (5.12)$$

Combining (5.11) and (5.12) with (5.9) and (5.10) the inverse- $\Gamma$  model is found to be

$$\mathbf{v}_{\alpha\beta s} - r_s \mathbf{i}_{\alpha\beta s} - L_\sigma \frac{d\mathbf{i}_{\alpha\beta s}}{dt} - L_M \frac{d\mathbf{i}_{\alpha\beta M}}{dt} = 0 \quad (5.13)$$

$$j\omega_r \Psi'_{\alpha\beta R} - r'_R \mathbf{i}'_{\alpha\beta R} - L_M \frac{d\mathbf{i}_{\alpha\beta M}}{dt} = 0. \quad (5.14)$$

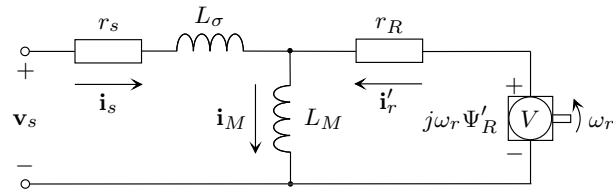


Figure 5.2: Dynamic inverse- $\Gamma$  equivalent circuit

When designing the current controller it is convenient to eliminate the rotor current from the equations, since it is usually not possible to measure

it. Instead the rotor flux linkage is used as a state variable together with the stator current. So, by substituting  $\mathbf{i}'_{\alpha\beta R} = \mathbf{i}_{\alpha\beta M} - \mathbf{i}_{\alpha\beta s}$  into (5.13) and (5.14) the dynamic inverse- $\Gamma$  model with rotor current eliminated is given by

$$L_\sigma \frac{d\mathbf{i}_{\alpha\beta s}}{dt} = \mathbf{v}_{\alpha\beta s} - (r_s + r'_R) \mathbf{i}_{\alpha\beta s} + \left( \frac{r'_R}{L_M} - j\omega_r \right) \Psi'_{\alpha\beta R} \quad (5.15)$$

$$\frac{d\Psi'_{\alpha\beta R}}{dt} = r'_R \mathbf{i}_{\alpha\beta s} - \left( \frac{r'_R}{L_M} - j\omega_r \right) \Psi'_{\alpha\beta R}. \quad (5.16)$$

Expressing the above inverse- $\Gamma$  model in synchronous ( $dq$ ) coordinates ( $d/dt \rightarrow d/dt + j\omega_e$ ) yields

$$L_\sigma \frac{d\mathbf{i}_{dqs}}{dt} = \mathbf{v}_{dqs} - (r_s + r'_R + j\omega_e L_\sigma) \mathbf{i}_{dqs} + \left( \frac{r'_R}{L_M} - j\omega_r \right) \Psi'_{dqR} \quad (5.17)$$

$$\frac{d\Psi'_{dqR}}{dt} = r'_R \mathbf{i}_{dqs} - \left( \frac{r'_R}{L_M} + j(\omega_e - \omega_r) \right) \Psi'_{dqR}. \quad (5.18)$$

The mechanical dynamics are described by (4.45), the electrical torque by (4.46) and the load torque by (4.54). In synchronous coordinates and inverse- $\Gamma$  form the equations can be written as

$$\frac{d\omega_r}{dt} = \frac{P}{2J} (T_e - T_L) \quad (5.19)$$

$$T_e = \left( \frac{3}{2} \right) \left( \frac{P}{2} \right) (\psi'_{dR} i_{qs} - \psi'_{qR} i_{ds}) \quad (5.20)$$

$$\omega_{mech} = \frac{2}{P} \omega_r. \quad (5.21)$$

### 5.3 Current Controller

As mentioned earlier, the synchronous ( $dq$ ) frame current controller is preferred since all electrical variables have DC steady-state values viewed from the synchronous frame. Zero steady-state error can be provided using only a simple PI-controller. However, in [5] it is suggested that to improve the dynamic performance the cross-coupling terms have to be eliminated since the dynamic response deteriorates as the synchronous frequency ( $\omega_e$ ) increases. The cross-coupling terms links the imaginary and real axis in (5.17) and are given by

$$j\omega_e L_\sigma \mathbf{i}_{dqs} \quad (5.22)$$

$$- (r'_R/L_M - j\omega_r) \Psi'_{dqR} \quad (5.23)$$

where (5.22) is the current  $dq$  axis cross-coupling term and (5.23) is the electromechanical cross-coupling term defined as the back e.m.f (i.e. the effect of rotor flux and velocity on the stator current ( $E$ )).

To cancel out the cross-couplings the following decoupler terms are used

$$j\omega_e \hat{L}_\sigma \mathbf{i}_{dqs} \quad (5.24)$$

$$j\omega_r \Psi'_{dqR} \quad (5.25)$$

where  $\hat{L}_\sigma$  is the estimated total leakage inductance and where the term  $r'_R/L_M$  is assumed to be much smaller than  $j\omega_r$ . The voltage equation (5.17) can be expressed as

$$\mathbf{v}_{dqs} = \tilde{\mathbf{v}}_{dqs} + j\omega_e \hat{L}_\sigma \mathbf{i}_{dqs} + j\omega_r \Psi'_{dqR}. \quad (5.26)$$

Assuming that there is an exact removal of the cross-coupling terms (i.e. the inductances have been estimated correctly) the system to be controlled is now a simple RL circuit. Using (5.17) and (5.26) it can be written as

$$L_\sigma \frac{d\mathbf{i}_{dqs}}{dt} = \tilde{\mathbf{v}}_{dqs} - (r_s + r'_R) \mathbf{i}_{dqs}. \quad (5.27)$$

Laplace transforming (5.27) gives

$$\tilde{\mathbf{G}}(s) = \frac{\mathbf{i}_{dqs}}{\tilde{\mathbf{v}}_{dqs}} = \frac{1}{sL_\sigma + r_s + r'_R} \quad (5.28)$$

which represents the system to be controlled using a PI controller on the form

$$\mathbf{F}_e(s) = k_{pe} + \frac{k_{ie}}{s} \quad (5.29)$$

where the controller parameters,  $k_{pe}$  and  $k_{ie}$  is determined using *internal model control* (IMC) [5]. The idea with IMC is to make the closed loop system into a first order low-pass filter, which is possible since  $\tilde{\mathbf{G}}(s)$  is of order one. The closed loop transfer function from  $\mathbf{i}_{dqs}^*$  to  $\mathbf{i}_{dqs}$  is given by

$$\mathbf{G}_{ce}(s) = \frac{\alpha_e}{s + \alpha_e} = \frac{1}{sT_e + 1} \quad (5.30)$$

where  $\alpha_e = 1/T_e$  is the closed loop bandwidth and  $T_e$  is the closed-loop time constant. For a first order system, the relation between rise time  $t_{re}$  and time constant  $T_e$ , alternatively the relation between bandwidth  $\alpha_e$  and rise time  $t_{re}$ , is given by

$$t_{re} = T_e \ln 9 \quad (5.31)$$

$$\alpha_e t_{re} = \ln 9. \quad (5.32)$$

Forming the closed loop transfer function from  $\mathbf{i}_{dqs}^*$  to  $\mathbf{i}_{dqs}$  using (5.28) and (5.29) yields

$$\mathbf{G}_{ce}(s) = \frac{\mathbf{F}_e(s) \tilde{\mathbf{G}}(s)}{1 + \mathbf{F}_e(s) \tilde{\mathbf{G}}(s)}. \quad (5.33)$$

Combining (5.33), (5.30) and (5.28) gives

$$\mathbf{F}_e(s) = \frac{\alpha_e}{s} \tilde{\mathbf{G}}^{-1}(s) = \alpha_e \hat{L}_\sigma + \frac{\alpha_e (\hat{r}_s + \hat{r}'_R)}{s}. \quad (5.34)$$

From (5.34) and (5.29) the controller parameters can easily be identified as

$$k_p = \alpha_e \hat{L}_\sigma \quad (5.35)$$

$$k_i = \alpha_e (\hat{r}_s + \hat{r}'_R). \quad (5.36)$$

### 5.3.1 Active Damping

The IMC designed controller will not be able to well suppress the load disturbance caused by the back emf. One idea [5] is to use *active damping* which means that a fictive resistance  $r_a$  is added to the already existing resistances  $r_s$  and  $r'_R$  in order to minimize the control error. The closed loop system from  $\tilde{\mathbf{v}}_{dqs}$  to  $\mathbf{i}_{dqs}$  is now given by

$$\tilde{\mathbf{G}}(s) = \frac{1}{sL_\sigma + r_s + r'_R + r_a} \quad (5.37)$$

With active resistance added, the integral part of the current controller has to be modified to yield  $k_i = \alpha_e (\hat{r}_s + \hat{r}'_R + r_a)$ . With  $r_a$  determined with the assumption that the inner feedback loop  $\tilde{\mathbf{G}}(s)$  is as fast as the outer feedback loop  $\mathbf{G}_{ce}(s)$ , i.e.  $(r_s + r'_R + r_a)/L_\sigma = \alpha_e \Rightarrow r_a = \alpha_e L_\sigma - (r_s + r'_R)$ , the controller parameters is determined according to

$$k_p = \alpha_e \hat{L}_\sigma \quad (5.38)$$

$$k_i = \alpha_e^2 \hat{L}_\sigma \quad (5.39)$$

### 5.3.2 Back Calculation

For large steps in the current reference signal, the current controller voltage output often exceeds the voltage limited by the power electronics. When this happens, the integrator part of the PI controller will build up an error called *integrator windup* due to the saturated voltage. The error can be quite large giving current overshoot during the time it takes the integrator to work off the error. To solve the problem a method called *back calculation* can be used. The idea is to define a new error signal for the integrator which gives a PI controller that never allows the voltage to exceed the voltage limit. The PI controller can be described by

$$\frac{dI}{dt} = e_e \quad (5.40)$$

$$\tilde{\mathbf{u}}_{dqs} = k_{pe} e_e + k_{ie} I \quad (5.41)$$

$$\tilde{\mathbf{v}}_{dqs} = \text{sat}(\tilde{\mathbf{u}}_{dqs}) \quad (5.42)$$

where  $\tilde{\mathbf{u}}_{dqs}$  is the ideal output signal and  $I$  is the integrator state variable. From (5.41) it can be seen that  $\bar{e}$  has to be selected as

$$\tilde{\mathbf{v}}_{dqs} = k_{pe}\bar{e}_e + k_{ie}I. \quad (5.43)$$

Combining (5.43) with (5.41) yields

$$\bar{e}_e = e_e + \frac{1}{k_{pe}}(\tilde{\mathbf{v}}_{dqs} - \tilde{\mathbf{u}}_{dqs}). \quad (5.44)$$

The control algorithm with back calculation can be written as

$$\frac{dI}{dt} = e_e + \frac{1}{k_{pe}}(\tilde{\mathbf{v}}_{dqs} - \tilde{\mathbf{u}}_{dqs}) \quad (5.45)$$

$$\tilde{\mathbf{u}}_{dqs} = k_{pe}e_e + k_{ie}I \quad (5.46)$$

$$\tilde{\mathbf{v}}_{dqs} = \text{sat}(\tilde{\mathbf{u}}_{dqs}). \quad (5.47)$$

### 5.3.3 Simulink Implementation

The current controller implemented in MATLAB/Simulink is a PI controller with active damping to suppress load disturbance and with back calculation to avoid integrator windup due to voltage saturation. The block diagram can be seen in Figure 5.3.

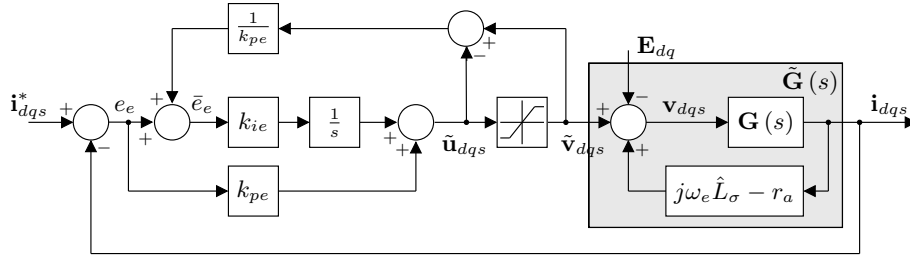


Figure 5.3: Current controller with decoupling, active damping and back calculation.

## 5.4 Speed Controller

The speed controller is designed in much the same way as the current controller, see section 5.3, including active damping to suppress the load disturbance  $T_L$  and back calculation to limit the current output signal.

The speed controller is designed assuming that the current controller is much faster, i.e.  $\alpha_e \ll \alpha_m$  and  $\mathbf{F}_e(s) = 1$ . The mechanical dynamics, defined by (4.45), is given by

$$J \frac{d\omega_{mech}}{dt} = T_e - T_{load} - b\omega_{mech} \quad (5.48)$$

where  $b$  is the viscous friction,  $P$  is the number of poles and  $T_{load}$  is the load torque defined in section 4.2.

With perfect field orientation the electrical torque  $T_e$ , defined by (4.46), can be written in inverse- $\Gamma$  synchronous coordinates as

$$T_e = \left(\frac{3}{2}\right) \left(\frac{P}{2}\right) \psi'_{dR} i'_{qR}. \quad (5.49)$$

The transfer function from  $T_e$  to  $\omega_{mech}$  is given by

$$G_m(s) = \frac{1}{sJ + b}. \quad (5.50)$$

Following the procedure in section 5.3 the speed controller parameters  $k_{pm}$  and  $k_{im}$  is found to be

$$F_m(s) = \frac{\alpha_m}{s} G_m^{-1}(s) = \frac{\alpha_m}{s} (sJ + b) = \alpha_m J + \frac{\alpha_m b}{s} \quad (5.51)$$

where

$$k_{pm} = \alpha_m \hat{J} \quad (5.52)$$

$$k_{im} = \alpha_m \hat{b}. \quad (5.53)$$

### 5.4.1 Active Damping

The active damping term introduced is given by

$$T_e = \tilde{T}_e - B_a \omega_{mech} \quad (5.54)$$

where  $B_a$  is the active damping constant. Inserting (5.54) into (5.48) and choosing the closed loop bandwidth  $\alpha_m$  as the pole of (5.48) instead of  $-b/J$ , the dynamics can be written as

$$\frac{d\omega_{mech}}{dt} = \frac{\tilde{T}_e}{J} - \underbrace{\frac{B_a + b}{J}}_{\alpha_m} \omega_{mech} - \frac{T_L}{J}. \quad (5.55)$$

Solving for  $B_a$  yields

$$B_a = \alpha_m \hat{J} - \hat{b}. \quad (5.56)$$

Including active damping the controller parameters (5.52) and (5.53) can be written as

$$k_{pm} = \alpha_m \hat{J} \quad (5.57)$$

$$k_{im} = \alpha_m^2 \hat{J}. \quad (5.58)$$



## 5.5 Flux Sensorless Control

The flux linkage is estimated using the equation for the rotor flux, (5.18). Assuming that  $\Psi_R$  is real-values, i.e. perfect field orientation, (5.18) can be simplified to yield

$$\frac{d\hat{\psi}'_{dR}}{dt} = \hat{r}'_R \hat{i}_{dqs} - \left( \frac{\hat{r}'_R}{\hat{L}_M} + j(\omega_e - \omega_r) \right) \hat{\psi}'_{dR}. \quad (5.65)$$

Separating the real and imaginary parts gives

$$\frac{d\hat{\psi}'_{dR}}{dt} = \hat{r}'_R i_{ds} - \frac{\hat{r}'_R}{\hat{L}_M} \hat{\psi}'_{dR} \quad (5.66)$$

$$\omega_e - \omega_r = \frac{\hat{r}'_R i_{qs}}{\hat{\psi}'_{dR}} \quad (5.67)$$

where the transformation angle is found by integrating the synchronous speed, i.e.

$$\theta_e = \int \omega_e dt. \quad (5.68)$$

### 5.5.1 Simulink Implementation

The flux estimator is implemented using (5.66) and (5.67). A block diagram representation of the equations can be seen in Figure 5.5.

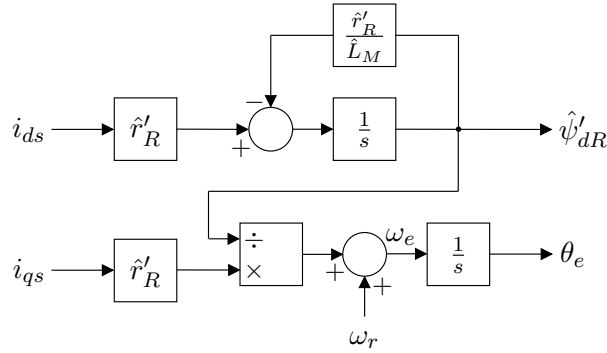


Figure 5.5: Flux linkage estimation.

## 5.6 Speed and Flux Sensorless Control

Sensorless control requires estimation of rotor speed and linkage flux. It is also assumed that the flux field is perfectly oriented along the d-axis.

### 5.6.1 Speed Estimation

Without a speed sensor the rotor speed has to be estimated. Writing (5.18) in component form yields

$$\frac{d\psi'_{dR}}{dt} = r'_R i_{ds} - \frac{r'_R}{L_M} \psi'_{dR} + (\omega_e - \omega_r) \psi'_{qR} \quad (5.69)$$

$$\frac{d\psi'_{qR}}{dt} = r'_R i_{qs} - \frac{r'_R}{L_M} \psi'_{qR} - (\omega_e - \omega_r) \psi'_{dR}. \quad (5.70)$$

With perfect field orientation ( $\psi'_{qR} = 0$ ) the  $q$ -direction rotor voltage (5.70) is found to be

$$0 = r'_R i_{qs} - (\omega_e - \omega_r) \psi'_{dR}. \quad (5.71)$$

By rearranging (5.71) the rotor speed estimate is found according to

$$\hat{\omega}_r = \omega_e - \frac{\hat{r}'_R i_{qs}}{\hat{\psi}'_{dR}}. \quad (5.72)$$

### 5.6.2 Flux Estimation

Combining (5.10) with (5.13) and rearranging, an expression for the rotor flux in the stationary reference frame is found. By integrating the same expression an estimate of the rotor flux can be found according to

$$\hat{\Psi}'_{\alpha\beta R} = \int (\mathbf{v}_{\alpha\beta s} - \hat{r}_s \mathbf{i}_{\alpha\beta s}) dt - \hat{L}_\sigma \mathbf{i}_{\alpha\beta s}. \quad (5.73)$$

Integration by a pure integrator ( $1/s$ ) of (5.73) give rise to drift and saturation problems [11]. To solve the problems, the integrator is replaced by a low-pass filter. The rotor flux estimate can now be written as

$$\hat{\Psi}'_{\alpha\beta R} = \frac{1}{s + \alpha} (\mathbf{v}_{\alpha\beta s} - \hat{r}_s \mathbf{i}_{\alpha\beta s}) - \hat{L}_\sigma \mathbf{i}_{\alpha\beta s} \quad (5.74)$$

or in a more compact form

$$\hat{\Psi}'_{\alpha\beta R} = \frac{1}{s + \alpha} \hat{\mathbf{E}}_{\alpha\beta} \quad (5.75)$$

where  $\hat{\mathbf{E}}_{\alpha\beta}$  is a voltage defined as  $\mathbf{v}_{\alpha\beta s} - \hat{r}_s \mathbf{i}_{\alpha\beta s} - \hat{L}_\sigma \frac{d\mathbf{i}_{\alpha\beta s}}{dt}$ .

For the stator flux to be estimated correctly, there must be a phase lag of  $90^\circ$  and a gain of  $1/|\hat{\omega}_e|$  since this is the space lag and gain of the pure integrator, see Figure 5.6. The above defined low-pass filter phase lag and gain,  $\phi$  and  $A$  respectively, is given by

$$\phi = -\tan^{-1} \left( \frac{\hat{\omega}_e}{\alpha} \right) \quad (5.76)$$

$$A = \left| \frac{\hat{\Psi}'_{\alpha\beta s}}{\mathbf{E}_{\alpha\beta}} \right| = \frac{1}{\sqrt{\hat{\omega}_e^2 + \alpha^2}}. \quad (5.77)$$

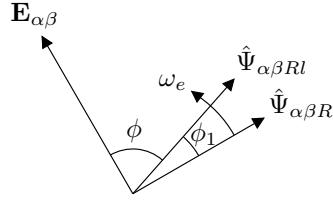


Figure 5.6: Vector diagram of low-pass filter and pure integrator.

Compensating for the space lag and gain using a gain compensator  $C_G$  and a phase compensator  $C_P$  given by

$$C_G = \frac{\sqrt{\hat{\omega}_e^2 + \alpha^2}}{|\hat{\omega}_e|} \quad (5.78)$$

$$C_P = e^{-j\phi_1} \quad (5.79)$$

the new integrator can be written as

$$\hat{\Psi}_{\alpha\beta s} = \frac{1}{s + \alpha} \frac{\sqrt{\hat{\omega}_e^2 + \alpha^2}}{|\hat{\omega}_e|} e^{-j\phi_1} \mathbf{E}_{\alpha\beta} \quad (5.80)$$

where  $\phi_1$  is the difference in phase between the pure integrator and the low-pass filter. The phase compensator (5.79) is found using the following relationship

$$e^{-j\phi_1} = \cos \phi_1 - j \sin \phi_1 \quad (5.81)$$

$$\cos \phi_1 = \frac{|\hat{\omega}_e|}{\sqrt{\hat{\omega}_e^2 + \alpha^2}} \quad (5.82)$$

$$\sin \phi_1 = \frac{\lambda \hat{\omega}_e}{\sqrt{\hat{\omega}_e^2 + \alpha^2}}. \quad (5.83)$$

To further minimize the stator flux estimation error the low-pass filter pole  $\alpha$  is chosen to vary proportionally to the speed, i.e.

$$\alpha = \lambda |\hat{\omega}_e| \quad (5.84)$$

where  $\lambda$  is a constant to be chosen.

Transforming (5.80) to the synchronous reference frame, using the relationship  $s \rightarrow s + j\omega_e$ , indirect field orientation (IFO) is obtained. The estimated rotor flux in synchronous coordinates is given by

$$\hat{\Psi}_{dqR} = \frac{1}{s + j\hat{\omega}_e + \alpha} \frac{\sqrt{\hat{\omega}_e^2 + \alpha^2}}{|\hat{\omega}_e|} e^{-j\phi_1} \mathbf{E}_{dq}. \quad (5.85)$$

Inserting (5.81) and (5.84) into (5.85) yields

$$\hat{\Psi}_{dqR} = \frac{1 - j\lambda\text{sign}\hat{\omega}_e}{s + j\hat{\omega}_e + \lambda|\hat{\omega}_e|} \underbrace{(e_d + je_q)}_{\mathbf{E}_{dq}} \quad (5.86)$$

where

$$e_d = v_{ds} - \hat{r}_s i_{ds} - \hat{L}_\sigma \frac{di_{ds}}{dt} + \hat{\omega}_e \hat{L}_\sigma i_{qs} \quad (5.87)$$

$$e_q = v_{qs} - \hat{r}_s i_{qs} - \hat{L}_\sigma \frac{di_{qs}}{dt} - \hat{\omega}_e \hat{L}_\sigma i_{ds}. \quad (5.88)$$

Assuming that the current controller is much faster than the flux estimator, the derivative of the stator currents in (5.87) and (5.88) can be neglected. The equations can be written as

$$e_d = v_{ds} - \hat{r}_s i_{ds} + \hat{\omega}_e \hat{L}_\sigma i_{qs} \quad (5.89)$$

$$e_q = v_{qs} - \hat{r}_s i_{qs} - \hat{\omega}_e \hat{L}_\sigma i_{ds}. \quad (5.90)$$

Splitting (5.86) into its real and imaginary part, and solving for  $\omega_e$  in the imaginary part, gives

$$\hat{\psi}_{dR} = \frac{e_d + \lambda\text{sign}(\hat{\omega}_e) e_q}{s + \lambda|\hat{\omega}_e|} \quad (5.91)$$

$$\hat{\omega}_e = \frac{e_q - \lambda\text{sign}(\hat{\omega}_e) e_d}{\hat{\psi}_{dR}} \quad (5.92)$$

$$\theta_e = \int \hat{\omega}_e dt \quad (5.93)$$

where  $\theta_e$  is the rotor flux angle used for transformations between the stationary ( $\alpha\beta$ ) reference frame and the synchronous ( $dq$ ) reference frame.

### 5.6.3 Simulink Implementation

By embedding (5.72) and (5.92) in a first-order low-pass filter, using the same  $\alpha_e$  bandwidth as the current control loop, the algebraic loop problem is avoided. The rotor speed is determined using

$$\hat{\omega}_r = \alpha_e \int \left( \frac{e_q - \lambda\text{sign}(\hat{\omega}_e) e_d}{\hat{\psi}_{dR}} - \frac{\hat{r}'_R i_{qs}}{\hat{\psi}'_{dR}} - \hat{\omega}_r \right) dt \Bigg|_{-\omega_{max}}^{\omega_{max}} \quad (5.94)$$

$$\hat{\omega}_e = \hat{\omega}_r + \frac{\hat{r}'_R i_{qs}}{\hat{\psi}'_{dR}} \quad (5.95)$$

where  $\hat{\omega}_r$  has been confined to the interval  $[-\omega_{max}, \omega_{max}]$  to prevent unrealistic large values. Typical values of  $\omega_{max}$  are  $1.2\omega_{rated}$  below base speed and  $3.5\omega_{rated}$  in the field-weakening region [5].

It is also a good idea to prevent  $\hat{\psi}'_{dR}$  from getting to small and risk division by zero. Using

$$\hat{\Psi}_{dR} = \int \left( e_d + \lambda \text{sign}(\hat{\omega}_e) e_q - \lambda |\hat{\omega}_e| \hat{\Psi}_{dR} \right) dt \Big|_{\psi_{min}}^{\psi_{max}} \quad (5.96)$$

$\hat{\Psi}_{dR}$  is confined to the interval  $[\psi_{min}, \psi_{max}]$ . This also prevents the flux level from growing beyond any reasonable bound. Recommended boundaries are  $[0.6\psi_{nom}, 1.0\psi_{nom}]$  during normal operation according to [5].

The block diagram implemented in MATLAB/Simulink can be seen in Figure 5.7.

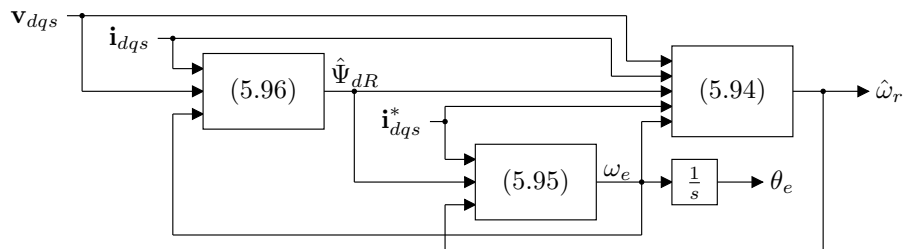


Figure 5.7: Simulink implemented flux and speed estimator.

# Chapter 6

## Verification

In this chapter the results are presented. The results consists of the parameters of the induction machine, verifying the induction machine model, the model for the washing machine drum with unbalanced load and finally the controller implementation.

### 6.1 Induction Machine

To be able to verify the induction machine model the tests described in section 4.1.1 have been performed. Due to limitations in the testing equipment the experiments have only been performed at 50Hz.

#### 6.1.1 T-Equivalent Circuit Parameters

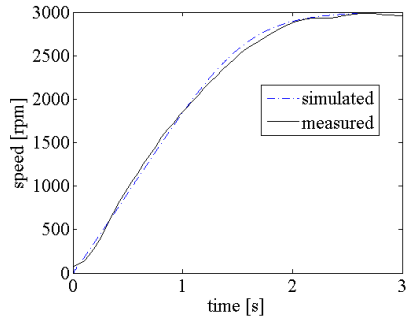
To determine the induction machine parameters the tests described in section 4.1.1 was performed. However, due to limitations in the test equipment the decision to ask the manufacturer for the parameters was made. The calculations made to determine the T-equivalent circuit parameters is found in Appendix G.

In addition to the T-equivalent circuit parameters, the inertia  $J$  of the induction machine is necessary when modelling. Using well known relations [12], the inertia was calculated to approximately  $0.55 \cdot 10^{-3} \text{ kgm}^2$  assuming that the rotor is made of solid iron.

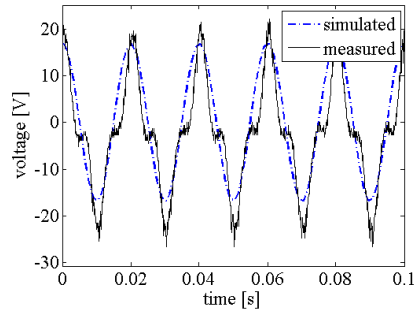
#### 6.1.2 Direct Start Measurements

The direct start measurements gives information about the transient behavior of the induction machine and is used to verify the induction machine model by comparing simulated with measured data. The direct start experiment, also described in section 4.1.1, was performed at 10V, 15V and 20V, all at 50Hz.

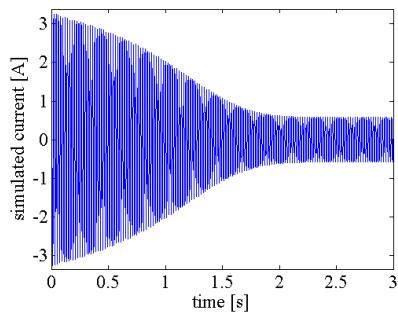
The result can be seen in Figure 6.1 to 6.3 and shows that the model is a very good representation of the real induction machine at all voltages tested.



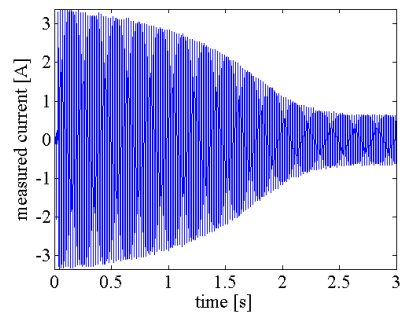
(a) Simulated and measured speed.



(b) Simulated and measured voltage.

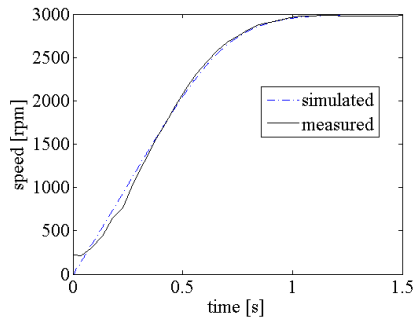


(c) Simulated current.

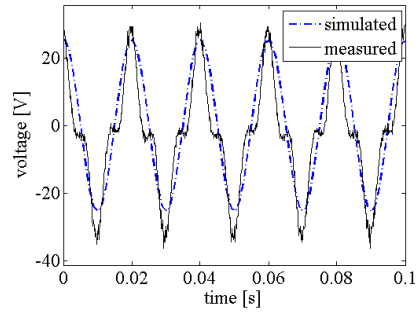


(d) Measured current.

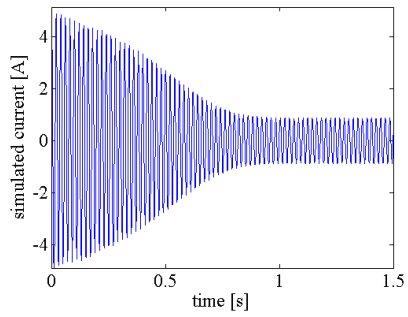
Figure 6.1: Simulated compared to measured data at 50Hz and  $12V_{\text{rms}}$ .



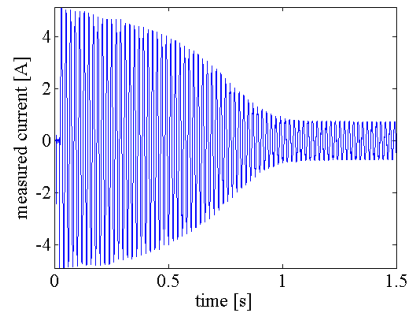
(a) Simulated and measured speed.



(b) Simulated and measured voltage.

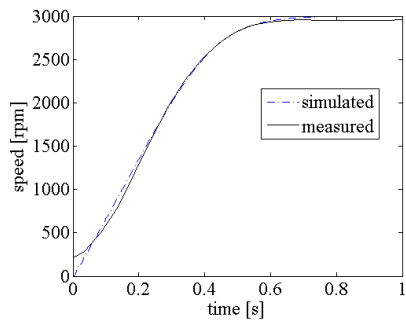


(c) Simulated current.

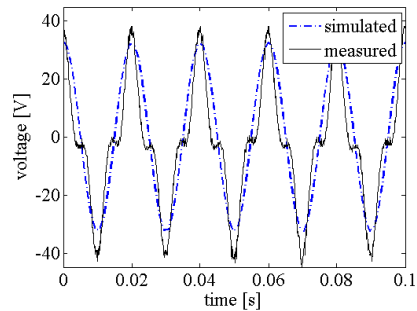


(d) Measured current.

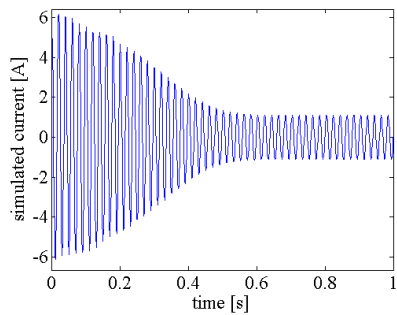
Figure 6.2: Simulated compared to measured data at 50Hz and  $18V_{\text{rms}}$ .



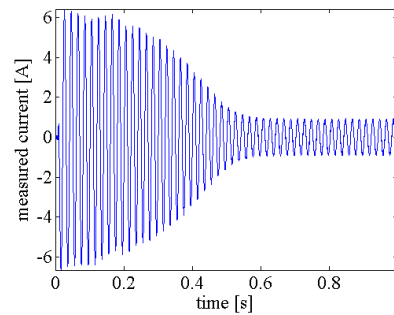
(a) Simulated and measured speed.



(b) Simulated and measured voltage.



(c) Simulated current.



(d) Measured current.

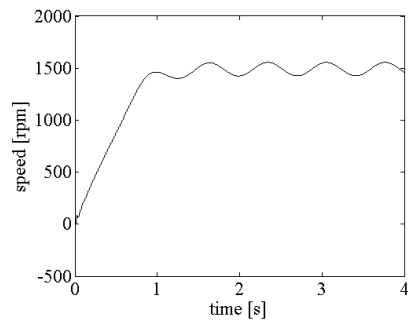
Figure 6.3: Simulated compared to measured data at 50Hz and  $23V_{\text{rms}}$ .

### 6.1.3 Induction Machine With Unbalanced Load

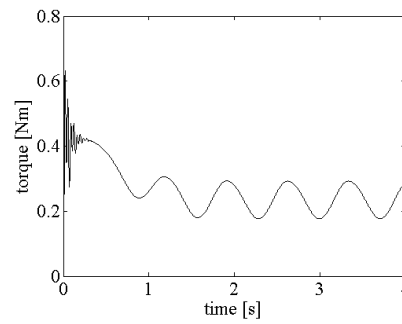
To verify the system consisting of the induction machine with unbalanced load a step in voltage was applied. As for the real washing machine, the unbalance measure was performed at a rotor speed of 1700rpm which results in a washing drum speed of approximately 100rpm.

The current, speed and load torque are shown in Figure 6.4 and 6.5 for unbalanced loads of 1000g and 3000g respectively. As can be seen in the figures there is a significant change in amplitude of the ripple when changing the mass of the unbalance load, both for speed and torque and as well for the stator current. With decreased unbalanced load mass the ripple is also decreased and is difficult to spot in the stator current represented in the  $abc$  reference frame. But, as can be seen in Figure 6.6, it is still quite easy to spot the ripples if the currents are being represented in the  $dq$  reference frame.

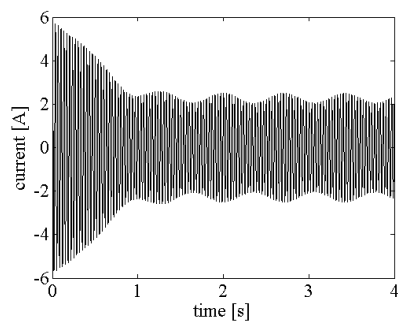
Finally, it should be mentioned that the drum model has not been experimentally verified and some of the parameters have been coarsely estimated, so the exact values from these simulations is not of interest.



(a) Rotor speed.



(b) Load torque.



(c) Stator current (one phase).

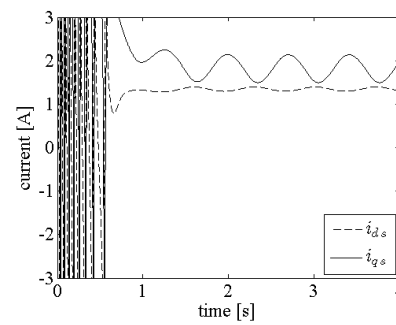
(d) Stator current in  $dq$  coordinates.

Figure 6.4: Speed, load torque and current with a 1000g unbalanced load.

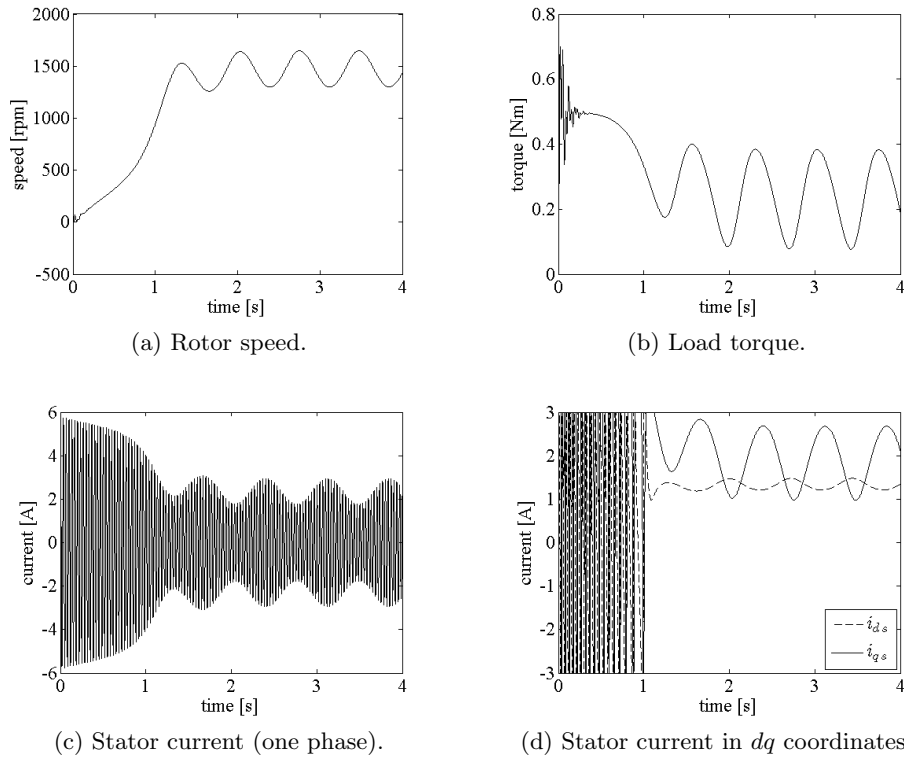


Figure 6.5: Speed, load torque and current with a 3000g unbalanced load.

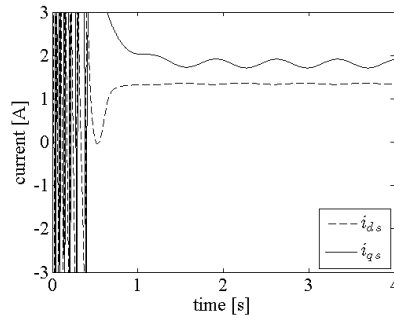


Figure 6.6: Current in  $dq$  coordinates with a 300g unbalanced load.

## 6.2 Drum

The unbalanced load detection on the real washing machine is performed at 100rpm. During this test the speed of the drum is ramped from 0 to 100rpm in one second with a unbalanced load mass of 1000g. The parameters for the drum, such as the inertia, the belt spring constant and the friction coefficient, have not been verified towards the real washing drum. Consequently, no exact conclusions can be drawn from the resulting plot, shown in Figure 6.7. However, the plot has the characteristic of an unbalanced load.

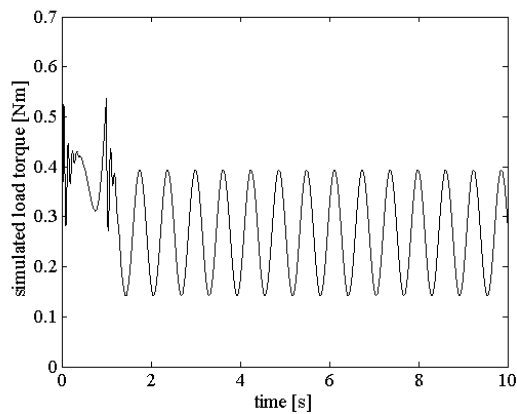


Figure 6.7: Load torque at 100rpm and 1000g unbalanced load

### 6.3 Current and Speed Controller

Two types of vector based controllers have been implemented in MATLAB/Simulink. The first is a flux sensorless, speed sensed controller, which is the typical situation in many induction machine drives, and the second a flux and speed sensorless controller, which is the ideal situation regarding cost and robustness.

#### 6.3.1 Flux Sensorless and Speed Sensed Control

Measuring the speed gives good performance at all speeds but the estimation of the flux angle is slightly more complicated compared to flux sensed control.

As can be seen in Figure 6.8 the rotor speed follows the reference speed in a satisfying way with a zero steady-state error. After five seconds a load torque of 1 Nm is applied, and as can be seen, the rotor speed makes a little dip before ending up at the desired rotor speed.

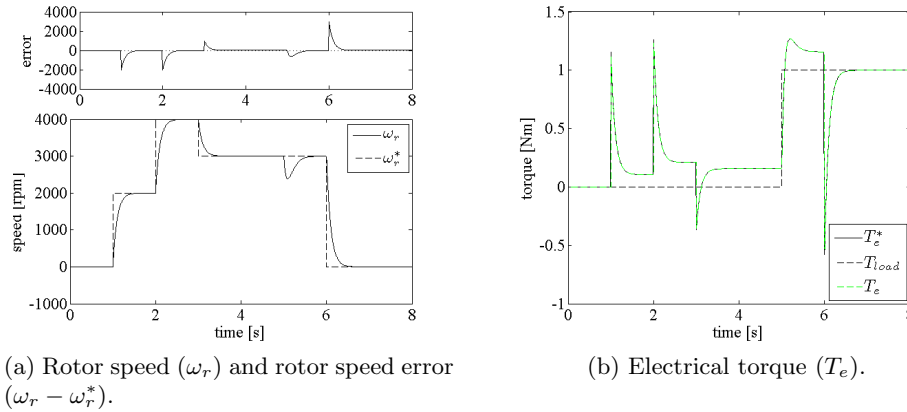


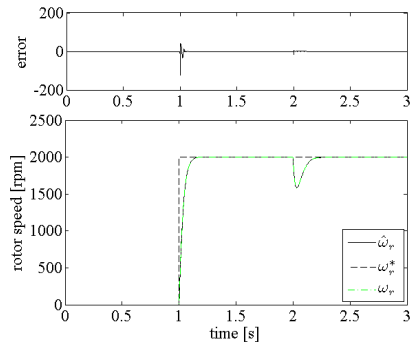
Figure 6.8: Flux sensorless control.

#### 6.3.2 Flux and Speed Sensorless Control

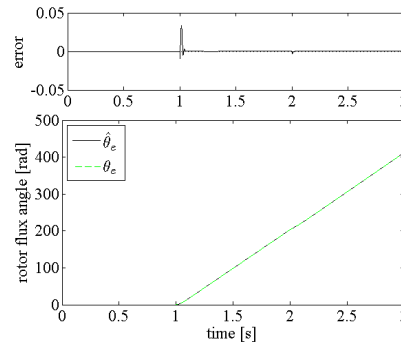
The actual value signals ( $\omega_r$ ,  $T_e$ ,  $\theta_e$  and  $\psi_{dR}$ ) are collected from the induction machine model, the estimate signals ( $\hat{\theta}_e$  and  $\hat{\psi}_{dR}$ ) are collected from the voltage model flux estimator (see Figure 5.1) and the reference signal ( $\omega_r^*$ ,  $T_e^*$  and  $\psi_{dR}^*$ ) are collected from the model input signals or from the controllers. In the simulation shown in Figure 6.9, the current controller bandwidth  $\alpha_e$  is set to 3000, the speed controller bandwidth  $\alpha_m$  is set to 30 and  $\lambda$  is set to 2.

A reference step in speed will result in transients which will damp out fast and give a zero steady-state error. It can be seen in Figure 6.9d that there

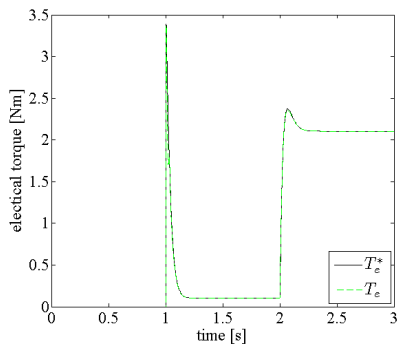
is an error in the flux during the magnetization of the machine. The error is due to that the derivative of the stator current is neglected in the equation determining the flux, i.e. (5.89) and (5.90). With perfect parameters there will be perfect load following.



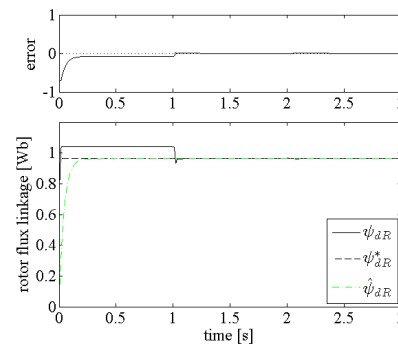
(a) Rotor speed ( $\omega_r$ ) and rotor speed error ( $\omega_r - \hat{\omega}_r$ ).



(b) Rotor flux angle ( $\theta_e$ ) and rotor flux angle error ( $\theta_e - \hat{\theta}_e$ ).



(c) Electrical torque ( $T_e$ ).



(d) Rotor flux linkage ( $\psi_{dR}$ ) and rotor flux linkage error ( $\psi_{dR} - \hat{\psi}_{dR}$ ).

Figure 6.9: Sensorless control using perfect parameters.

## Chapter 7

# Conclusion

A model of the induction machine that drives the washing machine drum, a model of the washing drum with unbalanced load and a speed and current controller have been derived and implemented in MATLAB/Simulink.

By determination of the T-equivalent circuit parameters using the motor supplier measurements, the induction machine model could be compared to the direct start measurements. As shown, the model represents the real induction machine in a satisfying way. It should be noted that due to limitations in the testing equipment, the direct start measurements have only been performed at 50Hz, and is thus the only frequency at which the induction machine model has been verified.

It was also noted that the unbalanced load had a significant influence on the stator currents, and that it was especially easy to see this if the currents were transformed to the synchronous ( $dq$ ) reference frame. Hence, it should be possible to draw conclusions of the mass of the unbalanced load from the sinusoidal shaped current variation. However, no conclusion of the exact mass can be drawn until the drum model with unbalanced load have been verified and all parameters, such as the friction coefficients and belt spring constant, have been determined.

Finally, two different controllers, both vector controlled, were derived and analyzed. The first controller is a flux sensorless, speed sensed drive which gives good performance at all speeds and is also a common way of controlling induction machines. The second controller is a flux and speed sensorless drive which requires a more complicated algorithm but is the ideal situation regarding cost and robustness [5]. At nominal speeds, a flux angle estimate of good accuracy can be obtained, but at low speeds it is difficult to guarantee stability and accuracy.

## Chapter 8

# Further Work

In this chapter some examples on further work, with the result of this thesis as a starting point, are presented. The suggestions for future thesis work includes

- The parameters for the drum, such as the belt spring constant and friction coefficients, is clearly subject for further work. Tests needs to be performed on a real washing machine to extract the parameters. To be able to draw further conclusions about the unbalanced load and the current variations in the stator the drum model with the unbalanced load also need to be verified.
- As presented in this thesis, it should be possible to determine the mass of the unbalanced load from the stator currents. So, one task could be to determine the mass of the unbalanced load by studying the stator currents represented in the synchronous reference frame. This could also include to investigate if it is possible to determine the position of the unbalanced load.
- If it is desirable to eliminate all sensors, other controller methods, such as DTC, could be investigated and compared to the sensorless vector controller presented in this thesis in order to find the most suitable controller.
- Finally, another machine of interest for further investigation is the permanent magnet synchronous machine (PMSM), which have some advantages over the induction machine in washer drives as discussed in [13].

# Nomenclature

$\alpha_e$	current controller bandwidth
$\alpha_m$	speed controller bandwidth
$\mu_1$	friction in rotor pulley
$\mu_2$	friction in drum pulley
$\omega$	angular speed in arbitrary reference frame
$\omega_1$	mechanical rotor speed
$\omega_e$	synchronous speed
$\omega_{mech}$	mechanical rotor speed, $(2/P)\omega_r$
$\omega_r$	electrical rotor speed
$\Psi'_{abcr}$	rotor flux vector referred to the stator
$\Psi_r$	rotor flux vector
$\Psi_s$	stator flux vector
$\mathbf{i}'_{abcr}$	rotor current vector referred to the stator
$\mathbf{i}_{abcr}$	rotor current vector
$\mathbf{i}_{abcs}$	stator current vector
$\mathbf{v}'_{abcr}$	rotor voltage vector referred to the stator
$\mathbf{v}_{abcr}$	rotor voltage vector
$\mathbf{v}_{abcs}$	stator voltage vector
$\xi$	belt spring constant
$b$	rotor friction coefficient
$B_a$	active damping friction coefficient

$d$	belt damping constant
$F_k$	belt force, $k = 1, 2$
$J$	rotor inertia
$J_1$	inertia of the rotor
$J_2$	inertia of the drum
$k_{ie}$	current controller integral gain
$k_{im}$	speed controller integral gain
$k_{pe}$	current controller proportional gain
$k_{pm}$	speed controller proportional gain
$L'_{lr}$	rotor leakage inductance referred to the stator
$L_\sigma$	transformed total leakage inductance, $L_s - L_M$
$L_{lr}$	rotor leakage inductance
$L_{ls}$	stator leakage inductance
$L_{mr}$	rotor magnetizing inductance
$L_{ms}$	stator magnetizing inductance
$L_M$	transformed magnetizing inductance, $L_m^2/L_r$
$L_m$	magnetizing inductance
$L_r$	rotor self-inductance, $L_m + L_{lr}$
$L_s$	stator self-inductance, $L_m + L_{ls}$
$n$	rotor speed [rpm]
$N_r$	number of rotor windings
$N_s$	number of stator windings
$n_s$	synchronous speed [rpm]
$P$	number of poles
$r'_r$	rotor resistance referred to the stator
$r_1$	rotor axis radius
$r_2$	drum radius

$r_a$	active damping resistance
$r_R$	transformed rotor resistance, $(L_m/L_r)^2 r_r$
$r_r$	rotor resistance
$r_s$	stator resistance
$s$	slip
$T_{\mu_k}$	torque due to friction, $k = 1, 2$
$T_e$	electrical torque
$T_{J_k}$	torque due to inertia, $k = 1, 2$
$T_k$	torque due to force on belt, $k = 1, 2$
$T_L$	load torque

# Bibliography

- [1] IEEE (1983). *IEEE Guide: Test Procedures for Synchronous Machines*, IEEE Std 115-1983. 22 Sept. E-ISBN: 0-7381-4332-4. <[www.ieee.org](http://www.ieee.org)>. (2007-04-24)
- [2] IEEE (2004). *IEEE Standard Test Procedure for Polyphase Induction Motors and Generators*, IEEE Std 112-2004. E-ISBN: 0-7381-3978-5. <[www.ieee.org](http://www.ieee.org)> (2007-04-24)
- [3] Ion Boldea, Syed A. Nasar (2002). *The Induction Machine Handbook*. Boca Raton: CRC Press. ISBN 0-8493-0004-5
- [4] A. Gastli (1999). Identification of induction motor equivalent circuit parameters using the single-phase test. *Energy Conversion, IEEE Transactions on*, vol. 14, issue 1, p. 51-56. ISSN: 0885-8969
- [5] Harnefors, Lennart (2002). *Control of Variable-Speed Drives*. Mälardalen: Department of Electronics Mälardalen University.
- [6] Krause, Paul et.al (2002). *Analysis of Electric Machinery and Drive Systems*. 2nd edition. Piscataway: IEEE Press. ISBN 0-471-14326-X
- [7] Briz del Blanco, Fernando et.al. (1999). *Dynamic Analysis of Current Regulators for AC Motors Using Complex Vectors*. Industry Applications, IEEE Transactions. vol. 35, pp. 1424-1432, Nov./Dec. 1999.
- [8] Hughes, Austin (2006). *Electric Motors and Drives*. 3rd edition. Oxford: Elsevier. ISBN 0-7506-4718-3
- [9] J. C. Trounce, S. D. Round, R. M. Duke. *Evaluation of Direct Torque Control using Space Vector Modulation for Electric Vehicle Applications*. University of Canterbury, New Zealand. <[http://www.elec.canterbury.ac.nz/research/powerelectronics/documents/AUPEC2001\\_DTC.pdf](http://www.elec.canterbury.ac.nz/research/powerelectronics/documents/AUPEC2001_DTC.pdf)> (2007-04-16)
- [10] ABB, Finland. Technical Guide No 1. Direct Torque Control. <<http://www.abb-drives.com/StdDrives/RestrictedPages/Marketing/Documentation/files/PProducts/DTC/TechGuide1.pdf>> (2007-04-16)

- [11] Myoung-Ho Shin et.al. (2000). *An Improved Stator Flux Estimation for Speed Sensorless Stator Flux Orientation Control of Induction Motors*. IEEE Transactions on power electronics vol. 15, no 2. mars 2000
- [12] Nordling, Carl. Österman, Jonny. (2004). *Physics Handbook*. Seventh edition. Lund: Studentlitteratur. ISBN: 91-44-03152-1
- [13] Murray, Aengus (2006). Sensorless Motor Control Simplifies Washer Drives. *Power Electronics Technology*.  
<<http://powerelectronics.com/mag/606PET20.pdf>> (2007-04-20)

## Appendix A

# Reference Frame Theory

It is preferable to derive the induction machine model in an arbitrary frame and later adapt the model to the preferred one depending on the problem to be solved. The same model can then be used solving different problems.

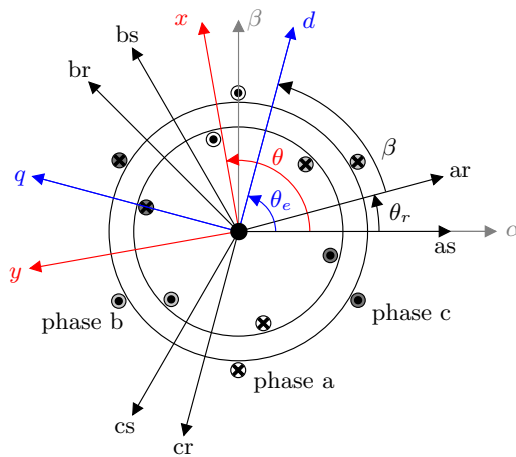


Figure A.1: Reference frames superimposed on a 3-phase induction machine.

The most commonly used reference frames are summarized in Table A.1 and shows the values taken by  $\theta$  and  $\beta$  shown in Figure A.1.

Reference Frame	$\theta$	$\beta$	Description
Rotor	$\theta_r$	0	The $xy$ axes rotate at rotor speed.
Stationary ( $\alpha\beta$ )	0	$-\theta_r$	The $xy$ axes do not rotate.
Synchronously rotating ( $dq$ )	$\theta_e$	$\theta_e - \theta_r$	The $xy$ axes rotate at synchronous speed.

Table A.1: Commonly used reference frames.

The following guidelines are suggested in [6] when choosing which reference frame to use

- Use the stationary reference frame if the stator voltages are either unbalanced or discontinuous and the rotor voltages are balanced.
- Use the rotor reference frame if the rotor voltages are either unbalanced or discontinuous and the stator voltages are balanced.
- Use either the stationary or synchronous reference frames if all voltages are balanced and continuous.

It is also suggested that the synchronously rotating reference frame may be useful in variable frequency applications. In this thesis, the stationary ( $\alpha\beta$ ) reference frame will be used for the induction machine model and the synchronous ( $dq$ ) reference frame will be used for the controller.

## A.1 Stationary Circuit Element

Transforming the stationary circuit elements from the 3-phase reference frame ( $abc$ ) to the arbitrary reference frame ( $xy$ ) (see Figure A.1) can be performed in two steps or in one single step. Transforming in two steps means that the  $abc$  frame first has to be transformed to the  $\alpha\beta$  frame and then from the  $\alpha\beta$  frame to the  $xy$  frame. The two step transformation is given by

$$\begin{bmatrix} f_{\alpha s} \\ f_{\beta s} \end{bmatrix} = \frac{2}{3} \begin{bmatrix} 1 & -\frac{1}{2} & -\frac{1}{2} \\ 0 & -\frac{\sqrt{3}}{2} & \frac{\sqrt{3}}{2} \end{bmatrix} \begin{bmatrix} f_{as} \\ f_{bs} \\ f_{cs} \end{bmatrix} \quad (\text{A.1})$$

$$\begin{bmatrix} f_{xs} \\ f_{ys} \end{bmatrix} = \begin{bmatrix} \cos \theta & \sin \theta \\ -\sin \theta & \cos \theta \end{bmatrix} \begin{bmatrix} f_{\alpha s} \\ f_{\beta s} \end{bmatrix} \quad (\text{A.2})$$

with the term  $2/3$  in (A.1) representing amplitude invariant transformation. Transforming back again yields

$$\begin{bmatrix} f_{\alpha s} \\ f_{\beta s} \end{bmatrix} = \begin{bmatrix} \cos \theta & -\sin \theta \\ \sin \theta & \cos \theta \end{bmatrix} \begin{bmatrix} f_{xs} \\ f_{ys} \end{bmatrix} \quad (\text{A.3})$$

$$\begin{bmatrix} f_{as} \\ f_{bs} \\ f_{cs} \end{bmatrix} = \begin{bmatrix} 1 & 0 \\ -\frac{1}{2} & -\frac{\sqrt{3}}{2} \\ -\frac{1}{2} & \frac{\sqrt{3}}{2} \end{bmatrix} \begin{bmatrix} f_{\alpha s} \\ f_{\beta s} \end{bmatrix}. \quad (\text{A.4})$$

Transforming from the stationary to the arbitrary frame, or reversed, can also be expressed as

$$\mathbf{f}_{xys} = \mathbf{f}_{\alpha\beta s} e^{-j\theta} \quad (\text{A.5})$$

$$\mathbf{f}_{\alpha\beta s} = \mathbf{f}_{xys} e^{j\theta}. \quad (\text{A.6})$$

To transform directly from the  $abc$  frame to the arbitrary frame (and the other way around) the following equations, where  $\mathbf{f}$  can represent current, voltage or flux linkage, are used

$$\mathbf{f}_{xy0s} = \mathbf{K}_s \mathbf{f}_{abc} \quad (\text{A.7})$$

$$\mathbf{f}_{abc} = (\mathbf{K}_s)^{-1} \mathbf{f}_{xy0s} \quad (\text{A.8})$$

where

$$\mathbf{f}_{xy0s} = [ f_{xs} \quad f_{ys} \quad f_{0s} ]^T \quad (\text{A.9})$$

$$\mathbf{f}_{abc} = [ f_{as} \quad f_{bs} \quad f_{cs} ]^T \quad (\text{A.10})$$

$$\mathbf{K}_s = \frac{2}{3} \begin{bmatrix} \cos \theta & \cos \left( \theta - \frac{2\pi}{3} \right) & \cos \left( \theta + \frac{2\pi}{3} \right) \\ -\sin \theta & -\sin \left( \theta - \frac{2\pi}{3} \right) & -\sin \left( \theta + \frac{2\pi}{3} \right) \\ \frac{1}{2} & \frac{1}{2} & \frac{1}{2} \end{bmatrix} \quad (\text{A.11})$$

$$(\mathbf{K}_s)^{-1} = \begin{bmatrix} \cos \theta & -\sin \theta & 1 \\ \cos \left( \theta - \frac{2\pi}{3} \right) & -\sin \left( \theta - \frac{2\pi}{3} \right) & 1 \\ \cos \left( \theta + \frac{2\pi}{3} \right) & -\sin \left( \theta + \frac{2\pi}{3} \right) & 1 \end{bmatrix} \quad (\text{A.12})$$

$$\omega = \frac{d\theta}{dt}. \quad (\text{A.13})$$

Note that a variable,  $f_{0s}$ , called the zero sequence component is included with the  $dq$  variables in order to handle unbalanced voltages and to be able to invert the transform  $\mathbf{K}_s$ .

### Resistive Elements

For a 3-phase resistive circuit, the following yields

$$\mathbf{v}_{abc} = \mathbf{r}_s \mathbf{i}_{abc}. \quad (\text{A.14})$$

Combining (A.8) with (A.14) the resistive circuit can be expressed in the arbitrary reference frame, i.e.

$$\mathbf{v}_{xy0s} = \mathbf{K}_s \mathbf{r}_s (\mathbf{K}_s)^{-1} \mathbf{i}_{xy0s}. \quad (\text{A.15})$$

Assuming a symmetrical induction machine, the resistance of each winding is the same ( $r_{sa} = r_{sb} = r_{sc} = r_s$ ) and the following is true

$$\mathbf{K}_s \mathbf{r}_s (\mathbf{K}_s)^{-1} = \mathbf{r}_s = \begin{bmatrix} r_s & 0 & 0 \\ 0 & r_s & 0 \\ 0 & 0 & r_s \end{bmatrix}. \quad (\text{A.16})$$

### Inductive Elements

For a 3-phase inductive circuit, the following yields

$$\mathbf{v}_{abc s} = \frac{d\Psi_{abc s}}{dt} = p\Psi_{abc s} \quad (\text{A.17})$$

As for the resistive circuit, the inductive circuit can also be expressed in the arbitrary reference frame by substituting (A.17) into (A.7), which gives

$$\begin{aligned} \mathbf{v}_{xy0s} &= \mathbf{K}_s p \left[ (\mathbf{K}_s)^{-1} \Psi_{xy0s} \right] \\ &= \mathbf{K}_s p \left[ (\mathbf{K}_s)^{-1} \Psi_{xy0s} \right] + \mathbf{K}_s (\mathbf{K}_s)^{-1} p \Psi_{xy0s}. \end{aligned} \quad (\text{A.18})$$

Combining (A.18) with well known trigonometric identities it can instead be expressed as

$$\mathbf{v}_{xy0s} = \omega \Psi_{yx0s} + p \Psi_{xy0s}. \quad (\text{A.19})$$

For a linear magnetic system, which is assumed in this theses, the flux linkages may be expressed as

$$\Psi_{abc s} = \mathbf{L}_s \mathbf{i}_{abc s} \quad (\text{A.20})$$

or expressed in the arbitrary reference frame

$$\Psi_{xy0s} = \mathbf{K}_s \mathbf{L}_s (\mathbf{K}_s)^{-1} \mathbf{i}_{xy0s}. \quad (\text{A.21})$$

The inductance matrix  $\mathbf{L}_s$  describes the relationship between the self- and mutual inductance,  $L_{ls}$  and  $L_{ms}$  respectively, of the stator phases of a symmetrical induction machine.

A winding self-inductance is the ratio of the flux linked by that winding to the current flowing in that winding with all other winding currents zero. Mutual induction is the ratio of flux linked by one winding due to current flowing in a second winding with all other winding currents zero including the winding for which the flux linkages are being determined (see for example [6] for detailed information about inductance relationship). The flux linkage for stator winding  $a$  can be written as

$$\begin{aligned} \psi_{as} &= (L_{ls} + L_{ms}) i_{as} - \frac{1}{2} L_{ms} i_{bs} - \frac{1}{2} L_{ms} i_{cs} + L_{sr} \cos \theta_r i_{ar} \\ &\quad + L_{sr} \cos \left( \theta_r + \frac{2\pi}{3} \right) i_{br} + L_{sr} \cos \left( \theta_r - \frac{2\pi}{3} \right) i_{cr} \end{aligned} \quad (\text{A.22})$$

where the same form yields for the flux linkages of stator winding  $b$  and  $c$  and for rotor winding  $a$ ,  $b$  and  $c$ . In matrix form the flux linkages are given by

$$\begin{bmatrix} \Psi_{abc s} \\ \Psi_{abc r} \end{bmatrix} = \begin{bmatrix} \mathbf{L}_s & \mathbf{L}_{sr} \\ (\mathbf{L}_{sr})^T & \mathbf{L}_r \end{bmatrix} \begin{bmatrix} \mathbf{i}_{abc s} \\ \mathbf{i}_{abc r} \end{bmatrix} \quad (\text{A.23})$$

where

$$\mathbf{L}_s = \begin{bmatrix} L_{ls} + L_{ms} & -\frac{1}{2}L_{ms} & -\frac{1}{2}L_{ms} \\ -\frac{1}{2}L_{ms} & L_{ls} + L_{ms} & -\frac{1}{2}L_{ms} \\ -\frac{1}{2}L_{ms} & -\frac{1}{2}L_{ms} & L_{ls} + L_{ms} \end{bmatrix} \quad (\text{A.24})$$

$$\mathbf{L}_r = \begin{bmatrix} L_{lr} + L_{mr} & -\frac{1}{2}L_{mr} & -\frac{1}{2}L_{mr} \\ -\frac{1}{2}L_{mr} & L_{lr} + L_{mr} & -\frac{1}{2}L_{mr} \\ -\frac{1}{2}L_{mr} & -\frac{1}{2}L_{mr} & L_{lr} + L_{mr} \end{bmatrix} \quad (\text{A.25})$$

$$\mathbf{L}'_{sr} = L_{ms} \begin{bmatrix} \cos \theta_r & \cos(\theta_r + \frac{2\pi}{3}) & \cos(\theta_r - \frac{2\pi}{3}) \\ \cos(\theta_r + \frac{2\pi}{3}) & \cos \theta_r & \cos(\theta_r + \frac{2\pi}{3}) \\ \cos(\theta_r + \frac{2\pi}{3}) & \cos(\theta_r - \frac{2\pi}{3}) & \cos \theta_r \end{bmatrix} \quad (\text{A.26})$$

$$(\text{A.27})$$

where  $L_{ms}$  is the mutual inductance of the stator winding,  $L_{ls}$  is the self-inductance of the stator winding,  $L_{mr}$  is the mutual inductance of the rotor winding,  $L_{lr}$  is the self-inductance of the rotor winding and  $L_{sr}$  is the mutual inductance between the stator and rotor windings.

## A.2 Rotating Circuit Element

Deriving the transformation matrices for the rotor is done in a similar manner as for the stationary circuit (see section A.1). The matrices defined for the rotating circuit element are thus only listed in this section. The matrices are given by

$$\mathbf{f}'_{xy0r} = [ f'_{xr} \quad f'_{yr} \quad f'_{0r} ]^T \quad (\text{A.28})$$

$$\mathbf{f}'_{abcr} = [ f'_{ar} \quad f'_{br} \quad f'_{cr} ]^T \quad (\text{A.29})$$

$$\mathbf{K}_r = \frac{2}{3} \begin{bmatrix} \cos \beta & \cos(\beta - \frac{2\pi}{3}) & \cos(\beta + \frac{2\pi}{3}) \\ -\sin \beta & -\sin(\beta - \frac{2\pi}{3}) & -\sin(\beta + \frac{2\pi}{3}) \\ \frac{1}{2} & \frac{1}{2} & \frac{1}{2} \end{bmatrix} \quad (\text{A.30})$$

$$(\mathbf{K}_r)^{-1} = \begin{bmatrix} \cos \beta & -\sin \beta & 1 \\ \cos(\beta - \frac{2\pi}{3}) & -\sin(\beta - \frac{2\pi}{3}) & 1 \\ \cos(\beta + \frac{2\pi}{3}) & -\sin(\beta + \frac{2\pi}{3}) & 1 \end{bmatrix} \quad (\text{A.31})$$

$$\omega_r = \frac{d\theta_r}{dt} \quad (\text{A.32})$$

$$\mathbf{r}_r = \begin{bmatrix} r_r & 0 & 0 \\ 0 & r_r & 0 \\ 0 & 0 & r_r \end{bmatrix}. \quad (\text{A.33})$$

## Appendix B

# DC Resistance Test

The stator winding resistance is preferably measured before any other test is performed since the resistance is dependent on the temperature. The experiment is conducted at room temperature which means that the resistance has to be corrected to yield during steady state performance. The following equation [1] can be used

$$R_t = R_{t_0} \frac{t + k}{t_0 + k} \quad (\text{B.1})$$

where  $k$  is the characteristic constant for the winding material,  $t$  is the limiting temperature according to the insulation classification,  $t_0$  is the temperature at which the experiment was conducted and  $R_{t_0}$  is the measured armature resistance at temperature  $t_0$ .

### Test Procedure

- Apply a DC voltage across two series connected phases. A relatively low value of current should be used so that the resulting  $I^2R$  loss will not cause a significant change in temperature during the time of application.
- Measure the current using a ampere-meter.
- Calculate the mean value of the stator winding resistance.

## Appendix C

### No-Load Test

The per phase equivalent circuit can be simplified at no-load to yield

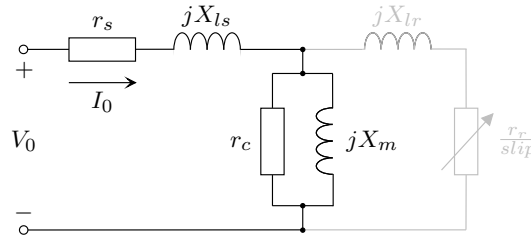


Figure C.1: Induction machine equivalent circuit at no-load.

With the motor connected to rated voltage and frequency and the rotor uncoupled from any mechanical load (i.e. the slip  $s$  is approximately equal to zero), the input power, current, frequency and voltage is noted to find the losses which in turn gives the magnetizing impedances ( $r_c$  and  $X_m$ ). The losses present are

- Hysteresis and Eddy current losses (iron losses) in stator ( $P_{Fe1}$ ) and rotor ( $P_{Fe2}$ )
- Winding and Friction losses ( $P_\mu$ )
- Copper losses in stator ( $P_{Cu1}$ ) and rotor ( $P_{Cu2}$ )

The total no-load loss can be described using

$$P_0 = P_{Fe1} + P_{Fe2} + P_{Cu1} + P_{Cu2} + P_\mu. \quad (\text{C.1})$$

At no-load,  $P_{Fe2}$  and  $P_{Cu2}$  (losses referred to the rotor) can be neglected and (C.1) can be written as

$$P_0 = P_{Fe1} + P_{Cu1} + P_\mu. \quad (\text{C.2})$$

The rotational losses comprises of iron losses and the windage and friction losses, i.e.

$$P_{rot} = P_{Fe} + P_{\mu} \approx P_{Fe1} + P_{\mu} = P_0 - P_{Cu1}. \quad (C.3)$$

The impedance (Figure C.1) of the magnetizing branch is found to be

$$Z_m = \frac{r_c j X_m}{r_c + j X_m} = \frac{r_c j X_m (r_c - j X_m)}{r_c^2 + X_m^2}. \quad (C.4)$$

With the assumption that  $X_m^2 \ll r_c^2$  (C.4) becomes

$$Z_m = \frac{X_m^2 + r_c j X_m}{r_c} = \frac{X_m^2}{r_c} + j X_m. \quad (C.5)$$

The resistive and reactive part of the above calculated impedance can now be used to find the total impedance

$$Z_0 = R_0 + j X_0 = \frac{V_0}{I_0} \quad (C.6)$$

$$R_0 = r_s + \frac{X_m^2}{r_c} = \frac{P_0 - P_{\mu}}{3I_0^2} \quad (C.7)$$

$$X_0 = X_{ls} + X_m = \sqrt{Z_0^2 - R_0^2}. \quad (C.8)$$

Since  $X_{ls}$  and  $X_m$  are not uniquely determined by the no-load test the value of the magnetizing reactance is determined using the the value of the stator leakage reactance derived in the locked rotor test, see Appendix D.

The magnetizing impedances can now be found by rewriting (C.7) and (C.8) according to

$$X_m = \sqrt{Z_0^2 - R_0^2} - X_{ls} \quad (C.9)$$

$$r_c = \frac{X_m^2}{R_0 - r_s} = \frac{3I_0^2 X_m^2}{P_0 - P_{\mu} - 3I_0^2 r_s}. \quad (C.10)$$

### Test Procedure

The no-load test is performed by running the machine at rated voltage and frequency without any load connected [2]. The iron loss will vary with the square of voltage while the friction loss will stay relatively constant because of constant motor speed. Adjusting the motor voltage and taking a series of readings from approximately 125% of rated voltage down to a minimum voltage where the motor current no longer drops with voltage the iron loss and the windage and friction loss can be determined.

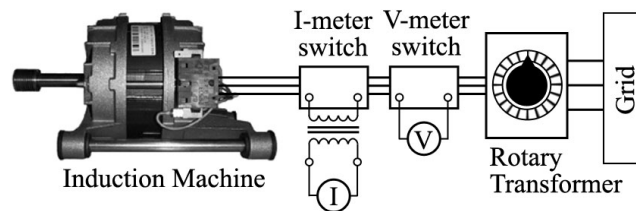


Figure C.2: Setup during no-load testing.

### Perform the following steps

1. Use the setup shown in Figure C.2 above.
2. Adjust the applied voltage to 125% of rated voltage.
3. Take readings of the line currents and voltages. The no-load current ( $I_0$ ) is taken as the average of the line currents. The same yields for the no-load voltage ( $V_0$ ).
4. Decrease the applied voltage and repeat step 3.

The no-load power ( $P_0$ ) is found, using the above measured currents and voltages, using

$$P_0 = S \cos(\varphi) \quad (\text{C.11})$$

where  $S = V_1 I_1 + V_2 I_2 + V_3 I_3$ . The phase angle  $\varphi$  is found by measuring the time instance of the peak of the phase voltage and current. The time difference is then referenced to the period of the waveform and converted to degrees. The following MATLAB code can be used to find the magnitude and phase position of a signal

```

signal      = v1;    % currents and voltages
fftvector   = fft(signal)/((length(signal))/2);
magnitudes  = abs(fftvector);
phaseshifts = 180/pi*atan2(imag(fftvector),real(fftvector));
position    = 51;   % this is for 50Hz and 1s sampling duration
magnitude(position) % get the magnitude
phasshift(position) % get the phase position

```

## Appendix D

# Locked Rotor Test

During this test, the rotor is at stand still, while low voltage is applied to stator windings to circulate the rated current. At this point, all of the power going to the motor is lost in the windings. This is the copper loss at full load. Initial test should be performed at maximum (rated) current. Subsequent tests are performed at successively lower currents.

Since there is no rotation, the slip equals 1, so,  $r_r/s = r_r$ .  $X_m$  and  $r_c$  is connected in a parallel manner with the impedance  $Z_r$  (i.e.  $r_r + jX_{lr}$ ), so the input current divides between the two paths. However, the reactance  $X_m$  and resistance  $r_c$  is very much larger than the impedance  $Z_r$ , so we neglect the small current through  $X_m$  and  $r_c$  and assume that the current flows only through  $Z_r$ . Now the equivalent circuit for the locked rotor test can be simplified as shown in Figure D.1.

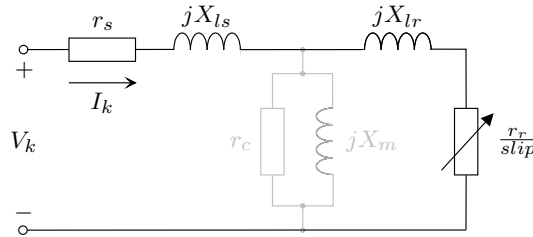


Figure D.1: Induction machine equivalent circuit with locked rotor.

The total impedance ( $Z_k$ ) can be calculated using the measured voltage ( $V_k$ ) and current ( $I_k$ ) according to

$$Z_k = \frac{V_k}{I_k}. \quad (\text{D.1})$$

The power factor ( $\phi_k$ ) is calculated using

$$\cos(\phi_k) = \frac{P_k}{3V_k I_k} \Rightarrow \phi_k = \arccos\left(\frac{P_k}{3V_k I_k}\right). \quad (\text{D.2})$$

The total resistance  $R_k$  and the total leakage reactance  $X_k$  can be derived using (D.1) and (D.2) according to

$$R_k = Z \cos(\phi_k) \quad (\text{D.3})$$

$$X_k = Z_k \sin(\phi_k). \quad (\text{D.4})$$

Knowing the total reactance  $Z_k$ , the frequency ( $\omega$ ) and assuming that  $X_{ls} \approx X_{lr}$ , the values of  $L_{ls}$  and  $L_{lr}$  can be calculated according to

$$X_{ls} = X_{lr} = \frac{X_k}{2} \quad (\text{D.5})$$

$$L_{ls} = \frac{X_{ls}}{\omega} \quad (\text{D.6})$$

$$L_{lr} = \frac{X_{lr}}{\omega}. \quad (\text{D.7})$$

With a cage motor the rotor resistance ( $r_r$ ) clearly cannot be measured directly, but the stator resistance ( $r_s$ ) can be obtained from a DC resistance test (as described in Appendix B) and hence the referred rotor resistance can be obtained using  $R_k = r_s + r_r$ .

If there is no flux saturation the locked rotor current varies directly with the voltage.

### Test Procedure

- Connect the induction motor and the DC motor with the torque meter in between them.
- Connect the DC motor to the thyristor converter and induction motor to the grid in the same way as in the no-load test shown in Figure C.2.
- Set the target speed for the DC motor speed controller to 0.
- Adjust the transformer to circulate rated current in induction motor.

Measure the voltage ( $V_k$ ), current ( $I_k$ ), input power ( $P_k$ ) and torque ( $T_{out}$ ) at different frequencies. Perform this test at successively lower voltage (current).

## Appendix E

# Direct Start

A direct start of a induction motor can be seen as a step in voltage. This test is done to achieve a reference for the simulation and hence to verify the derived model of the motor. During the direct start the current, voltage and speed is recorded and saved.

To determine the rotor inertia a current step is applied to the motor and the acceleration and torque applied can be used to derive the inertia. To record test data a computer is required.

The acceleration ( $\frac{d\omega}{dt}$ ) and the inertia ( $J$ ) is read from the measurement and the torque ( $T$ ) is calculated according to

$$T = J \frac{d\omega}{dt}. \quad (\text{E.1})$$

Another possibility is to measure the torque with a special meter connected between the induction motor and the break. The torque per phase can also be calculated using

$$T = \frac{1}{\omega_s} \frac{V_{as}^2}{(r_s + \frac{r_r}{s})^2 + X_l^2} \frac{r_r}{s} \quad (\text{E.2})$$

which yields only at steady-state.

The nomenclature is taken from Figure D.1 where  $X_l$  is the total reactance of  $X_{ls}$  and  $X_{lr}$ . The synchronous speed ( $\omega_e$ ) is calculated according to

$$\omega_e = \frac{2 \times 2\pi f}{P}. \quad (\text{E.3})$$

### Test Procedure

The set up for the voltage step test and the current step test is identical and done using the same set up as in the no load test described in Appendix C. In addition, if a torque meter is available this can be used to measure the

torque directly on the shaft. The torque meter is connected in between the induction motor and the break. The computer should be connected to be able to measure voltage, current, speed and torque.

**Voltage step**

- Start recording.
- Switch on the voltage supply.

**Current step**

In this test a current controller must be used. This can be implemented in the computer or in an external controller.

- Make sure the current controller is adjusted to the desired value.
- Start the recording.
- Start the current controller and make the step.

## Appendix F

# Torque-Speed Test

The torque-speed test is performed to find the operating characteristics of the electric machine. The resulting curve can then be used to match application with the appropriate machine. However, in this thesis the resulting torque-speed curve is used for Simulink model verification.

### Test Procedure

The torque-speed curve measurements are made using the same setup as for the locked rotor test, see Appendix D. At selected frequencies in the range from 0 to 380Hz, the voltage is adjusted so that the  $V/f$  ratio is kept constant until the base speed ( $\omega$ ) is reached by varying the load ( $T_L$ ) using the DC machine. Beyond base speed, full voltage should be applied while still varying the load until no-load is reached.

The following steps should be performed in order to obtain the torque-speed curves at frequency ranging from 0 to 380Hz:

1. Start with a frequency of 10 Hz and apply voltage accordingly, as described above ( $V/f = 0.5$ ).
2. Adjust the DC machine so that full load torque is achieved ( $s = 1$ ).
3. Measure the motor speed ( $\omega$ ) using the tachometer and the torque ( $T_L$ ) using the torque-meter.
4. Ease the breaking torque in steps.
5. Repeat step 3 and 4 until no-load is achieved ( $s = 0$ ).
6. Repeat step 2 to 5 above for frequencies up to the maximum of 380 Hz.

## Appendix G

# Induction Machine Parameters

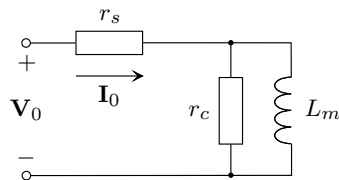
The T-equivalent circuit parameters for AHV CIM motor 10109 T is determined by using measured data supplied by the manufacturer ATB SELNI and the equations defined in Appendix C and D. The calculated data is then compared to the manufacturer calculated  $\Gamma$  model parameters.

### DC resistance

Parameter	Value
$r_s$	$2.65\Omega$

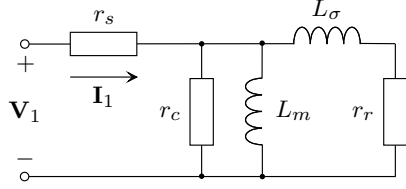
Table G.1: Measured per phase DC resistance data supplied by motor manufacturer.

### No-load



Parameter	Value
$P_0$	53.80W
$P_{Fe}$	45.68W
$Q_0$	258.10W
$I_0$	1.75A
$V_0$	150.64V

Figure G.1: Measured per phase no-load data supplied by motor manufacturer.

**Locked rotor**

Parameter	Value
$P_1$	34.47W
$P_r$	15.6W
$Q_1$	46.00W
$I_1$	2.67A
$V_1$	21.55V

Figure G.2: Measured per phase locked rotor data supplied by motor manufacturer.

**Calculations**

As described in Appendix D the inductances  $L_{ls}$  and  $L_{lr}$  and the rotor resistance  $r_r$  can be calculated using the measured locked rotor data. Using the equations defined in Appendix D,  $L_{ls}$ ,  $L_{lr}$  and  $r_r$  can be determined.  $L_m$  and  $r_c$  can be found using the no-load measurements together with expressions for the active and reactive power [3], which is given by

$$P_0 = \left( r_c \frac{X_m^2}{X_m^2 + r_c^2} + r_s \right) I_0^2 \quad (\text{G.1})$$

$$Q_0 = \left( X_m \frac{r_c^2}{X_m^2 + r_c^2} + X_{ls} \right) I_0^2. \quad (\text{G.2})$$

No-load		Locked rotor	
Parameter	Value	Parameter	Value
$\phi_0$	86.10°	$Z_k$	8.083Ω
$I_m$	1.746A	$\phi_k$	53.13°
$I_c$	0.119A	$R_k$	4.850Ω
$L_m$	0.0889H	$X_k$	6.467Ω
$r_c$	455Ω	$X_{ls}$	3.233Ω
		$X_{lr}$	3.233Ω
		$L_{ls}$	3.43mH
		$L_{lr}$	3.43mH
		$r_r$	2.2Ω

Table G.2: Calculated T-equivalent circuit parameters.

The T-equivalent circuit is given by

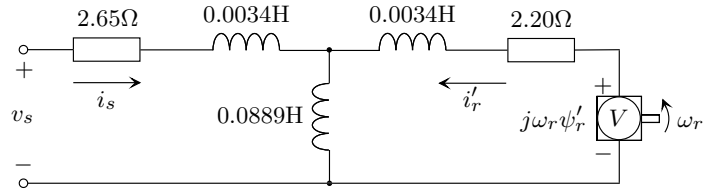


Figure G.3: T-equivalent circuit.

The parameters in the T-equivalent circuit above can be translated to  $\Gamma$  model parameters [4] which is the model used by the manufacturer. In this way the parameters can be verified.

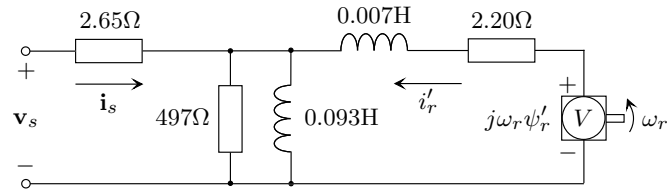


Figure G.4: Manufacturer calculated  $\Gamma$  model.